DISLOCATION DIPOLES AND LOOPS IN SINGLE CRYSTALS OF MAGNESIUM OXIDE

A Thesis Submitted
In Partial Fulfilment of the Requirements
for the Degree of
DOCTOR OF PHILOSOPHY

by

GUNUPUDI KAMESWARARAO

TH
PHY/1979/D
K128d

to the
DEPARTMENT OF PHYSICS
INDIAN INSTITUTE OF TECHNOLOGY KANPUR
1979 JULY

PHY-1974-D-KAM-DIS

CENTRAL LIBRARY
Acc. No. A 62236
13 MAY 1980

POST GRADUATE OFFICE
I.I.T Kanpur.
Submitted on 19...7 1979
BP

Department of Physics
Indian Institute of Technology
Kanpur, U.P., India

This is to certify that the work reported in this thesis has been carried out in this Department under my supervision. No part of this work has been submitted elsewhere for a degree.

(A S Parasnis)
Professor of Physics

1979.07.09

ACKNOWLEDGEMENTS

I am very much indebted to Professor A S Parasnis for introducing me to this field of research, suggesting the problem and guiding me throughout the course of the investigation. I am grateful to him for allowing me to make use of his suggestions in Chapter 5 and helping me in the preparation of this Report.

I thank the Director, IIT Kanpur for providing the facilities to carry out research work. I am grateful to Professors T M Srinivasan, T R Ramachandran, R K Ray, P Venkateswarlu, S C Agarwal, Sudhir Sen, D C Khan and S C Sen for the kind interest they took in my progress and for encouraging me. I wish to express my heartfelt gratitude to Dr K N Swamy Rao who helped me both academically and otherwise.

I am thankful to many of my friends who lent a helping hand in the preparation of the thesis. Dr P K Mishra and M/s J K Sharma and A K Nigam did a very careful proof reading of the typed script. M/s Mukul Misra, P K Srivastava, G V Rao, B Sairam, Prasanna and Kaushik helped in one way or the other. I am extremely thankful to my former colleague, Mr J M Mauskar for keeping me in

good spirits during testing times in the laboratory hours of work. I also thank Dr S K Chaturvedi who was not just a friend but a philosopher and guide too.

Special mention must be made of Mr J N Sharma, Foreman, Central Glass Shop, for the advice and innumerable suggestions rendered in overcoming many a technical hurdle during experimentation. I am very much grateful to him. My sincere thanks are due to Mr Ram Mangal Singh, of the Physics Workshop, who has been instrumental in executing many of my designs with great precision. Mr Ramesh Chandra Misra provided everyday laboratory assistance.

I thank the members of the technical staff of the Department of Physics who assisted in their respective spheres.

I thank the CSIR, New Delhi for the award of a research fellowship during the period 1973 (Jan) to 1975 (Dec).

This task would not have been possible but for the emotional support provided by my parents and brothers and sisters.

Finally, I am thankful to Mr Nihal Ahmad for his excellent typing, to Mr Lalloo Singh Rathaur for cyclostyling and to Mr A K Ganguly for preparing the drawings.

CONTENTS

Chapter	Section	Title	Page
		Table of Magnification of Photo-micrographs	vii
		Synopsis	viii
1		CHARGED DISLOCATIONS IN IONIC CRYSTALS	1
	1.1	Introduction	1
	1.2	Dislocations in Rocksalt Structure	2
	1.3	Charged Dislocations	4
	1.4	Alkali Halides	5
	1.5	Silver Halides	6
	1.6	Magnesium Oxide	6
	1.7	Motivation for the Present Work	8
2		EXPERIMENTAL METHODS	14
	2.1	Introduction	14
	2.2	Specimen Preparation	16
	2.2.1	{001}-Sections	17
	.2	{110}-Sections	17
	.3	Specimen cleaning	19
	2.3	Heat Treatment and Doping	19
	2.3.1	GLOBAR furnace	21
	.2	Platinum furnace	21
	.3	Molybdenum furnace	25
	.4	Thermal diffusion of gold	29
	2.4	Observational Techniques	32
	2.5	Micro-hardness Measurements	33
3		OBSERVATIONS	34
	3.1	Introduction	34
	3.1.1	As-received specimens	37
	3.2	Appearance of the Crystal Surface	38
	3.3	Decoration	40
	3.4.1	Colour of the crystals	44
	.2	Micro-hardness measurements	45
	3.5	Less Slowly Cooled Specimens	46
	3.5.1	Long and narrow dislocation loops	47
	.2	Eiffel towers	56
	.3	Somewhat unusual configurations	64
	3.6	Less Rapidly Cooled Crystals	69
	3.7	Previous Work on Dislocations in MgO	73

4		REVIEW OF DISLOCATION DIPOLES AND LOOPS IN SINGLE CRYSTALS OF MAGNESIUM OXIDE	77
	4.1	Introduction	77
	4.1.1	Slip in MgO	77
	.2	Suitability of MgO for dislocation studies	78
	4.2	Mechanisms of Formation of Dislocation Loops in MgO	79
	4.2.1	Aggregation of point defects mechanism	79
	.2	Dislocation dipole mechanism	80
	4.3	Dislocation Configurations Observed in MgO	89
	4.4	Summary	93
	4.5	Comment on the term 'Dipole'	95
5		DISCUSSION	97
	5.1	Approach	97
	5.2	Decoration	99
	5.3	Hardness	102
	5.4	Cooling Rate and Dislocation Configurations	103
	5.5	Eiffel Towers and Long and Narrow Loops	105
	5.5.1	Vacancy condensation	105
	.2	Dislocation collisions	106
	.3	Slip loops	106
	.4	Mechanism suggested	107
	.5	Loops L1b and L2b	120
	.6	Equilibrium of the helix of Figure 5.4	120
	5.6	Other Features	122
	5.6.1	Spikes	122
	.2	Lenticular loops and helix	122
	.3	Straight-segmented loops	122
	5.7	Concluding Remarks	123
APPENDIX A		PLATELETS	125
		REFERENCES	129

Table of Magnifications of Photomicrographs

Figure No	Magnification	Figure No	Magnification
3.1	600 ×	3.17(a,b)	935 ×
3.2	600 ×	3.18	1540 ×
3.3	230 ×	3.19(a,b)	1540 ×
3.4	935 ×	3.20	1540 ×
3.5(a,b)	935 ×	3.21	935 ×
3.6(a,b)	935 ×	3.22(a,b,c)	1540 ×
3.7(a,b)	935 ×	3.23(a,b)	1540 ×
3.8(a,b)	1540 ×	3.24	1540 ×
3.9(a,b,c)	1540 ×	3.25	1540 ×
3.10	935 ×	3.26	1540 ×
3.11	935 ×	3.27	1540 ×
3.12(a,b,c)	935 ×	A.1	600 ×
3.12d	1540 ×	A.2	375 ×
3.12e	935 ×	A.3	600 ×
3.15	1540 ×	A.4	600 ×
3.16(a,b)	935 ×		

SYNOPSIS

Name	Gunupudi Kameswararao
Degree	Ph D
Name of the Institution	Indian Institute of Technology Kanpur
Month and Year	July 1979
Title of the Thesis	DISLOCATION DIPOLES AND LOOPS IN SINGLE CRYSTALS OF MAGNESIUM OXIDE

This thesis reports studies on dislocations in single crystals of magnesium oxide (MgO), in particular dislocation dipoles and loops. It is divided into five chapters and one Appendix.

Chapter 1 gives the motivation for the study in the light of the present knowledge of charged dislocations in ionic crystals. It is now known that many effects in the plastic deformation of ionic solids (in particular, the alkali halides, zinc sulphide, ice) are connected with the fact that dislocations in them can be charged. In this chapter a distinction is drawn between dislocations which carry charges as a result of the precipitation of indigeneous point defects and those which carry purely configurational charges. It had been speculated that since the latter dislocations tend to follow unusual slip systems such crystals as contained them might have their mechanical properties modified in the event of the activation of such slip systems. The present work further strengthens this idea.

In Chapter 2 all the experimental procedures followed and techniques used are described. An account is given of the methods of sample preparation, and of the design and fabrication of high temperature (about 1800°C and 2200°C) furnaces which have platinum or molybdenum heating elements respectively. Observational methods (optical microscopy and micro-hardness testing) also are dealt with. In view of the very high melting point (2800°C) of magnesium oxide special methods of incorporating the impurity into the crystals were evolved. Gold was chosen as the impurity for reasons explained in Chapter 1. Heat treatment of specimens consisted in high temperature annealing and one- or two-stage cooling.

Detailed observations made by optical microscopy on heat-treated crystals are presented in Chapter 3. Observations were made on specimens of crystallographically different orientations prepared from doped and heat-treated {001}-blocks of crystal. They are illustrated with photomicrographs. Micro-hardness measurements were also made on the above sections. The major interest was in dislocation dipoles and loops; however, observations on oriented crystalline precipitates formed on the surfaces of crystals are also presented (Appendix A). The conditions of heat

treatment which tended to give rise to these dislocation configurations are described.

Dislocation dipoles and loops have been observed in single crystals of magnesium oxide by many previous workers who have identified the loops to be of prismatic in character. Those observed in the present work seem to be quite different. Hence attention has been concentrated on them. Various different kinds of loops (long and narrow; wide; straight-segmented; unusual) have been observed. The most interesting are long (125 μm) and narrow (<1.6 μm) loops; they do not seem to be prismatic. The earlier stages of the formation of these loops are observed to be in the form of the Eiffel Tower. The plane of the 'towers' is either {100} or {110}, whereas the legs of the base lie in parallel {110}-planes and are along different <112>-directions.

A brief review of earlier relevant work on dislocations in single crystals of magnesium oxide is given in Chapter 4. Since the present investigation concentrated on dipoles and loops the review is concerned with the mechanisms of formation of dipoles and loops rather than the totality of the dislocation interactions in and mechanical properties of magnesium oxide.

In Chapter 5 is given a complete analysis of the observations. It is concluded that the long-narrow loops and the straight-segmented loops are not formed by the collapse of discs of vacancies or the aggregation of interstitials into discs. It is argued that the dipoles that the Eiffel Towers are and the long-narrow loops are unlikely to have formed by any of the mechanisms described in Chapter 4. A new mechanism based on the zigzagging, with configurationally charged <112>-zigs and -zags, of an initially straight (length along either <110> or <100>) and neutral (a/2)<110> dislocation is suggested comprehensively to explain the existence of both {100} and {110} loop-planes, and of both <100> and <110> directions of elongation in the case of either loop-plane. Other observations also are discussed.

Chapter 1

CHARGED DISLOCATIONS IN IONIC CRYSTALS

1.1 Introduction

It is a known fact that dislocations in ionic crystals carry charges which influence the mechanical and electrical properties of the crystals. A few reviews have appeared in the past (Friedel 1964, Smolouchowski 1966, Nabarro 1967, Hirth and Lothe 1968). More recently Whitworth(1975) has given an exhaustive account, the first one ever, of charged dislocations in ionic crystals. He has dealt in detail with dislocations which have acquired charges but which are otherwise neutral. Sprackling (1976) has given some of the more elementary geometrical aspects in fair detail. Either the charged dislocations are directly observed or their effects are studied. While the former gives a qualitative idea about the structure and crystallography of charged dislocations, the latter study gives quantitative results regarding the magnitude and sign of the charge carried by the dislocations. The present investigation was initiated to make direct observations on charged dislocations in

single crystals of magnesium oxide. A brief review of some aspects of the charged dislocations in ionic crystals is given in this chapter and is followed by an account of the motivation for the present work.

1.2 Dislocations in Rocksalt Structure

Crystals of rocksalt structure usually glide on $\{110\}\langle 1\bar{1}0\rangle$-slip systems. $\{001\}\langle 1\bar{1}0\rangle$-systems are activated at high temperatures or with the decrease in the ionicity of the bond; for example, PbS and PbTe prefer gliding on $\{001\}\langle 1\bar{1}0\rangle$-slip systems to gliding on $\{110\}\langle 1\bar{1}0\rangle$. The extra half-planes of the $\{110\}\langle 1\bar{1}0\rangle$-edge dislocations are $\{1\bar{1}0\}$-planes terminating with two rows of ions of opposite signs, with the dislocation line lying along $\langle 001\rangle$. Ideally this dislocation is neutral and does not carry any charge. Acquisition by it of charged defects like jogs and of point defects leads to a charged state. In 1951 Mott and Seitz suggested independently that each half jog carries a charge of magnitude e/2.

Next we consider $\{111\}\langle 1\bar{1}0\rangle$-slip systems. In rocksalt structure a stacking based on $\{111\}$-planes consists of alternate layers of cations and anions. Slip in the usual $\langle 1\bar{1}0\rangle$-direction introduces an edge dislocation along $\langle 11\bar{2}\rangle$-direction with an extra half-plane consisting

of alternate strips of anions and cations terminating with a row of ions all of the same sign (Parasnis et al 1963). This dislocation carries a linear charge density given by

$$\lambda = \pm 2\sqrt{(2/3)} \cdot ez/a$$

where e is the electronic charge, a the lattice parameter and z the valency of the ion. This would give rise to a large electrostatic energy which is why dislocations do not follow this slip system normally.

Slip along <100>-direction is not favoured because in the mid-glide position like ions come nearer and large electrostatic repulsive forces would be created. Recently Narayan (1978a) has observed a<100>-dislocation loops in magnesium oxide. Since these have been identified as being of the vacancy type no actual slip is involved.

The relaxed positions of the ions around the edge dislocation so as to have minimum energy around the core were calculated by Huntington et al (1955). Based on these calculations Whitworth (1965) has drawn the diagram of the edge dislocation in NaCl crystal. Arain and Pugh (1968) performed similar calculations and obtained the ionic positions for a number of ionic solids (KCl, LiF, NaBr, MgO etc). The results of MgO are similar to those

of NaCl and hence the core structure of the edge dislocation in MgO will be similar to that of NaCl. Fontaine (1968) and Fontaine and Haasen (1969) have given a model of the edge dislocation core splitting up into partials bounding a stacking fault in between. There is as yet no direct evidence for the existence of stacking faults in ionic crystals (see Evans and Langdon 1976). Our view is that Fontaine's results simply imply that the core of the dislocation is rather wide.

1.3 Charged Dislocations

Stepanov (1933) observed a transient change in the ionic conductivity of NaCl while performing an experiment to detect the rise in temperature due to plastic deformation, even in the absence of electric field. The potential difference produced between the electrodes was correctly explained after two decades by Fishbach and Nowick (1955) as being due to the movement of charged dislocations. Many experiments were performed to observe the electrical effects and the signs of the charged dislocations. When these charged dislocations glide, because the ionic movements are along the Burgers vector, the charge is transported in the direction of Burgers vector by one or another mechanism (Whitworth 1975). The measurement of the charge has been made by subjecting a crystal to

indentation tests, bending tests, cyclic stress or compressive deformation. Electrodes are fixed on appropriate surfaces of the crystal and the electrical signals reaching the electrodes are measured. A number of workers have performed such experiments on a variety of crystals and the sign of the charge has been determined in all these cases.

1.4 Alkali Halides

Dislocations in alkali halides of nominal purity carry negative charge at room temperature. In divalent anion-doped crystals (like Na_2O_2-doped NaCl) and in pure crystals at high temperatures the charge was found to be positive. Studies on charged dislocations were concentrated mainly on alkali halides because of their availability in the purest form. A large number of experiments with different concentrations of impurity content has been carried out and quantitative measurements of the charge made. Rueda and DeKeyser (1961b) gave a value of charge on dislocations in pure sodium chloride crystals as $(1.39\pm0.13)\times10^{-11}$ C/cm and in doped sodium chloride crystals (0.6% $CdCl_2$ added in melt) as $(1.66\pm0.05)\times10^{-11}$ C. Galustashvili (1970) has determined the charge density on dislocations in lithium fluoride crystals doped with dominant anion and cation

impurities as being 3.3×10^{-14} C cm^{-1}, 1.4×10^{-13} C cm^{-1} in the case of anion-doped lithium fluoride and -2.0×10^{-13} C cm^{-1} in predominantly cation doped lithium fluoride crystals. De Batist et al (1968) obtained the charge density on dislocations in pure caesium iodide crystals at room temperature as about 3.0×10^{-16} C cm^{-1}.

1.5 Silver Halides

In silver halides the intrinsic defects are of Frenkel type unlike alkali halides which possess Schottky defects. Dislocations in intrinsic crystals carry positive charges in most of the cases. In extrinsic crystals doped with divalent cation impurities so as to have cation vacancies the dislocations carry negative charges. Because of their photographic properties they have been investigated with great interest. It was suggested that the charge on the dislocations plays an important role in the formation of the latent image.

1.6 Magnesium Oxide

Magnesium oxide has the rocksalt structure. Because the anions and cations are divalent the charge carried by the jogs, kinks and point defects is twice that of those in alkali halides. Rueda and Dekeyser (1961a) measured the charge of the dislocations in magnesium oxide from

indentation experiments and found it to be positive. These results could not be relied upon for the reason that it is not possible to grow magnesium oxide crystals as pure as the alkali halides. Also the observation, stated earlier, of positively charged dislocations in anion doped alkali halides indicates that the above result needs a cautious approach. Because the anions and cations in magnesium oxide are divalent it can have both monovalent and trivalent impurities. When MgO is doped with monovalent impurity, one impurity ion will occupy a substitutional position and another an interstitial one replacing a single ion of the matrix. On doping with a trivalent impurity, two impurity ions will replace three host ions leaving a vacancy with them. Thus a vacancy is associated with the impurity. Although ⟨100⟩-slip is electrically impossible as it introduces electrostatic faulting (Buerger 1930), recent observation of a<100> -dislocation loops by Narayan (loc cit) in magnesium oxide shows that further studies on charged dislocations in these crystals are needed.

Other materials investigated are CaF_2, UO_2, Ice, Ge, Si, etc.

1.7 Motivation for the Present Work

It was stated in §1.2 that the edge dislocation in the $\{111\}\langle 1\bar{1}0\rangle$-slip system lies along the $\langle 11\bar{2}\rangle$-direction. As pointed out by Parasnis (1960) and Parasnis *et al* (1963), the extra half-plane terminates with a strip of ions of the same sign (see Figures 1.1(a,b)). Thus, the edge dislocation in this slip system possesses its own charge, the configurational charge, unlike the $\{110\}\langle 1\bar{1}0\rangle$-dislocations which acquire charges from charged point defects. Because this introduces a large electrostatic energy this slip system was thought to be unobservable, even though there are crystals with fluorite structure which prefer gliding on the system, $\{100\}\langle 1\bar{1}0\rangle$, which introduces such a configurational charge. Parasnis (*loc cit*) observed in crystals of silver chloride containing cupric chloride rhombus-shaped prismatic dislocation loops having Burgers vector $(a/2)\langle 1\bar{1}0\rangle$. The sides of the rhombic loops were along $\langle 11\bar{2}\rangle$-directions indicating that these edge segments forming a loop lie on $\{111\}$-slip planes. Another important observation was a possible evidence indicating that the dislocations were capable of gliding on $\{111\}$-planes, rather than getting pinned down. As mentioned earlier these $\langle 11\bar{2}\rangle$ dislocations carry large electrostatic energy which is an appreciable fraction (20%) of elastic energy. This extra charge could

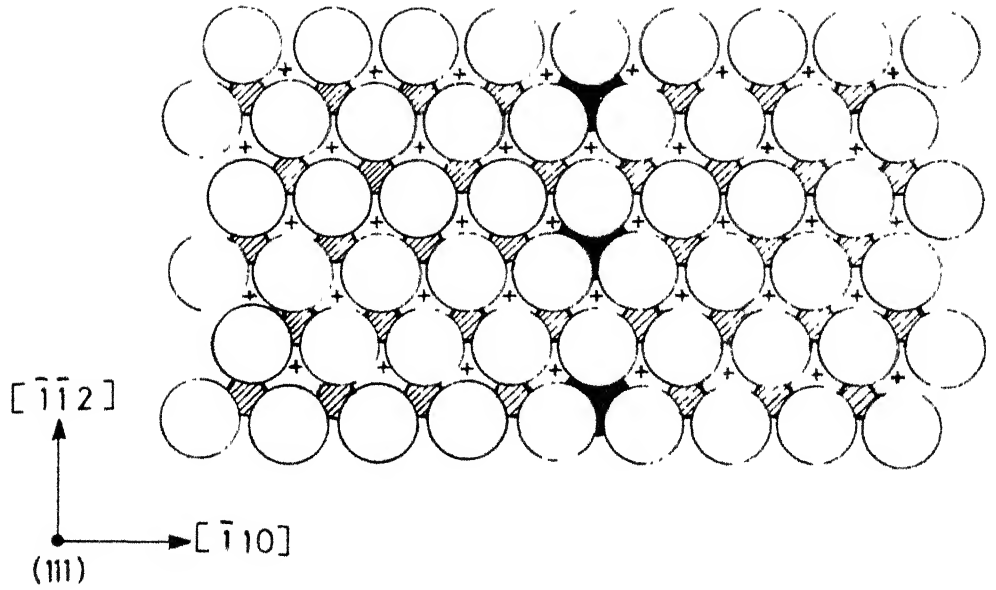

Figure 1.1a {111}<1$\bar{1}$0>-edge dislocation in the plane of the paper

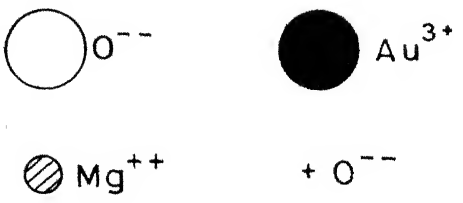

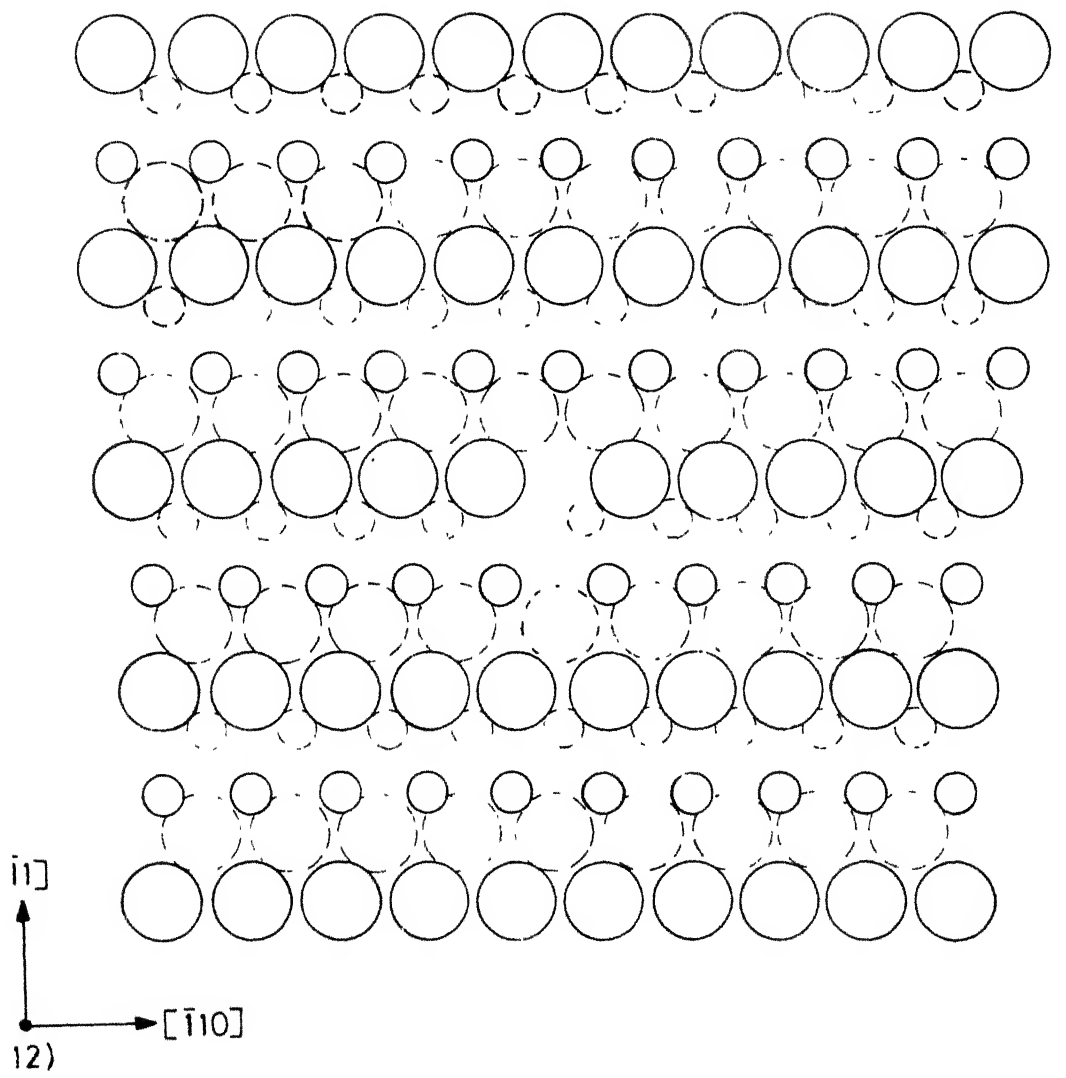

Figure 1.1b {111}<1$\bar{1}$0>-edge dislocation perpendicular to the plane of the paper

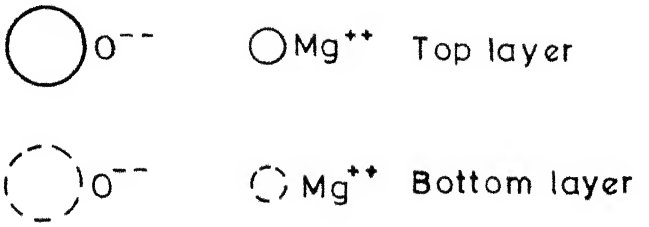

be neutralized (Parasnis *et al*, *loc cit*) if the terminating strip of the extra half-plane consisted of a strip of anions and the next strip of Ag^{+} and Cu^{++} cations alternately. Whereas Whitworth has discussed such configurationally charged dislocations in the fluorite structure he has failed to take notice of such dislocations in the rocksalt structure.

Around 1928 von Mises had proposed that for a polycrystal to undergo uniform homogeneous deformation it should possess five independent slip systems. von Mises gave a simple way of finding out whether the slip systems are independent or not by forming the determinant of the strain components (Groves and Kelly 1963b). Groves and Kelly have given a geometric interpretation of the von Mises result. For a polycrystalline material to undergo plastic deformation without the formation of voids along the grain boundaries the adjacent grains should accommodate the strains. This requires each grain to possess five independent slip systems. When five independent slip systems are not available voids are formed during plastic deformation of polycrystals. Kocks (1958) has studied the polyslip of polycrystals, *i e* simultaneous glide of dislocations in many slip systems of each grain, and in his words his results "..... seem to strengthen the concept of polyslip as being the one important mechanism of the plasticity of fcc polycrystals...".

In the rocksalt structure the commonly observed slip system is $\{110\}\langle 1\bar{1}0\rangle$ while $\{001\}\langle 1\bar{1}0\rangle$-slip system is activated at high temperatures. Even though these primary and secondary slip systems (as they are called) provide five independent slip systems, crystals of rocksalt structure do not exhibit polycrystalline ductility. Bicrystals of magnesium oxide tested in tension develop cracks along the boundary indicating that the boundary cannot accommodate the strains of the adjoining grain (Johnston et al 1962, Westwood 1961, Evans and Langdon 1976). The number of active slip systems in crystals of rocksalt structure is limited by the ionic character of the crystals. As mentioned earlier in § 1.2, slip on $\{111\}$-planes introduces configurationally charged dislocations and slip along $\langle 100\rangle$-directions causes electrostatic faulting. If we could devise suitable methods to offset these electrostatic effects it should be possible to expect the operation of such slip.

It was stated above that the neutralization of the configurational charge carried by $\{111\}\langle 1\bar{1}0\rangle$-dislocations in rocksalt structure had been possible in silver halides. In that case cupric ions were substituted for silver ions at alternate sites along the terminal strip. This effectively immobilizes the dislocation which would not then

contribute to plasticity. The basic requirement for the activation of this slip system is not only the neutralization of the extra charge but also that the neutralization be achieved without immobilizing the dislocation. Only then will the straight edge <112>-dislocation glide. Such a proposal has been made by Parasnis (1979) and is used in §§5.2.2 and 5.5.4.

Thus these investigations on magnesium oxide were initiated to study the possible activation of new slip systems and their effect on the mechanical properties.

Chapter 2

EXPERIMENTAL METHODS

2.1 Introduction

It was mentioned in Chapter 1 that the study on charged dislocations has been done in two ways, viz (i) estimation of the charge of the dislocations by detecting the electrical signals induced by their movement, and (ii) direct observation of the charged dislocations. The former method applies to the study of charges acquired by a dislocation which is otherwise neutral while the latter applies only to configurationally charged dislocations. The latter method was chosen in the present investigation as our objective was to study the possibility of activating the $\{111\}\langle 1\bar{1}0\rangle$-slip systems.

Dislocations in crystals are observed by one of the three methods, viz optical microscopy (etch pits, birefringence, decoration), electron microscopy, and x-ray topography. The very first direct observation of the dislocations was made by the decoration technique (Hedges and Mitchell 1953). Dislocations in single crystals of magnesium oxide were observed by Washburn et al (1960a) by transmission electron microscopy for the first time. This work initiated extensive investigations on this material. Venables (1961)

observed dislocations decorated by impurities and identified the decorating particles as ZrO_2 (1963). Bowen (1963) and Bowen and Clarke (1963) observed impurity precipitates associated with dislocations. Miles (1965) was the first to identify under the optical microscope dislocations decorated by the impurities, probably ZrO_2, in as-received as well as heat-treated crystals. Hendersen (1964) observed incoherent impurity precipitates associated with dislocations. Zakharov et al (1975) observed dislocation loops formed on FeO particles in as-grown crystals under TEM. Parasnis et al (1973) decorated the dislocations in single crystals of magnesium oxide by thermally diffusing gold. The present investigation is a continuation of that work performed with some improvements and in greater detail. Before going over to the details of the experimentation it would be worthwhile here to mention the mechanism of the decoration process (see Mitchell 1962).

The decoration process needs an appropriate cooling rate. Cooling always produces a supersaturation of vacancies which causes the dislocations to undergo climb. Decoration occurs during the cooling cycle of the heat treatment. First, particles are nucleated in the dislocation-free regions of the crystal and grow in size. These precipitate particles set up stress fields around them. These stress

fields are relaxed by the generation or annihilation of Schottky defects. Because of this the equilibrium concentration of the defects, which would be present at that temperature during cooling, is altered. To restore the equilibrium of the point defects the dislocations, which have not been decorated so far, undergo climb and take up different equilibrium configurations. The impurities nucleate along the cores of the dislocations and grow. Thus it is that the cooling rate must be programmed carefully.

2.2 Specimen Preparation

The crystals used in these experiments were obtained from commercial sources in USA. Single crystals of reasonably pure magnesium oxide in the form of rods with the cylindrical axis approximately along <001>-direction were obtained from Semi-Elements Inc, U.S.A.; and the randomly oriented blocks of single crystal were obtained from Ventron Corporation, USA. Thin sections (0.5 mm) parallel to {001}- and {110}-faces were prepared out of these bulk crystals by cleaving or slicing followed by mechanical grinding and polishing. Chemical polishing by hot orthophosphoric acid gives rather poor surface for optical microscopy. However, since {110}-specimens were usually too small to be ground and polished mechanically, they had to be polished chemically.

2.2.1 {001}-Sections

Not all of the crystals obtained from Semi-Elements had their axes along [001]-direction. Therefore, for convenience, only crystals of which the axes were along [001]-direction were made use of in preparing (001)-sections. These crystals were cleaved into thin discs (0.5 mm thick). They were then ground and polished with finer grades of alumina powder successively. The final polishing was done over pitch using cerium oxide as the abrasive. Specimens from the Ventron block crystals were prepared by cleaving with a chisel and hammer into rectangular blocks of size 3x3x10 mm^3. These were further cleaved into thin slices 0.5 mm thick.

2.2.2 {110}- Sections

{110}-Sections were prepared either directly from Semi-Elements cylindrical crystals or from the cleaved blocks of Ventron. The axes of the former were only nominally [001]. A jig (Figure 2.1) was fabricated to prepare {110}-sections taking into account the deviation α of the cylinder axis from [001]. This angle α varied from crystal to crystal. Therefore separate jigs were made corresponding to each deviation angle α. The crystal was mounted in the jig in such a way that its [100]- and [010]-axes coincided with those of the jig; by taking repeated back-reflection Laue photographs and applying the correction each time it was

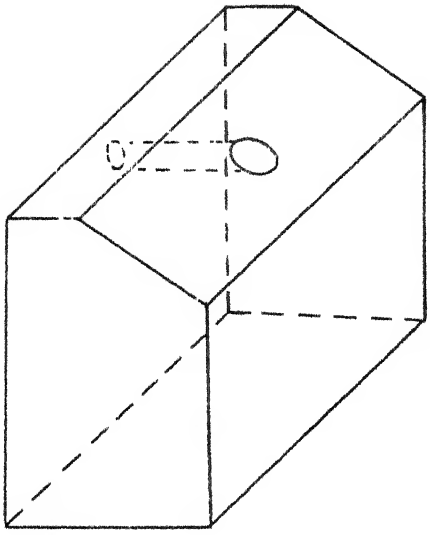

Figure 2.1 Jig for preparing (110)-sections

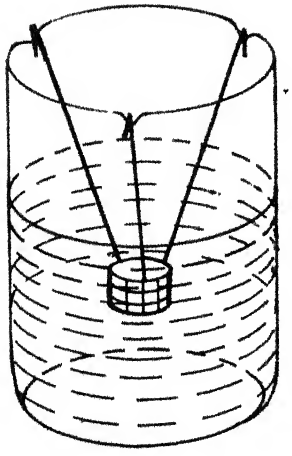

Figure 2.2 Glass basket to suspend the crystals for ultrasonic cleaning

correctly oriented. Once the crystal was correctly oriented it was fixed *in situ* by applying pitch on the plane face of the jig through which the crystal had been inserted. The jig was then held in a vice keeping the slanting face vertical. The crystal was then sliced with a tungsten wire saw along the slanting face. {110}-Sections were sliced by pushing the crystal forward after each cut. Before making each successive cut a back-reflection Laue photograph of the exposed face was taken and corrections were applied, if necessary. These {110}-sections were ground and polished in the same way as {001}-sections. (However, see §2.4 .)

2.2.3 Specimen cleaning

Once the specimens were polished they were cleaned with acetone in an ultrasonic cleaner. For the purpose of suspending the specimens during this cleaning a small glass basket was made (Figure 2.2). After this the specimens were cleaned with methanol.

2.3 Heat Treatment and Doping

As stated in §2.1 above, Miles (1965) had observed decorated dislocation configurations in as-received as well as simply heat-treated crystals of magnesium oxide, the decorating particles being of the impurities present in the as-received

crystals, very probably, as concluded by him, ZrO_2. As stated in Chapter 1, the purpose of diffusing gold was not simply to decorate the dislocations, but to activate new slip systems which give rise to configurationally charged dislocations. Parasnis et al (1973) decorated the dislocations by thermally diffusing gold at about 1400°C. But the decoration was rather faint and dislocation configurations could not be studied exhaustively. Therefore, in the present investigation the heat treatment procedure was reprogrammed on the basis of the two factors. (1) As mentioned in §2.1, the cooling rate is the controlling factor for good decoration. (2) Decoration experiments in the case of alkali and silver halides have always been performed at temperatures about 100°C below the melting point (Amelinckx 1957, Bartlett and Mitchell 1958, Parasnis and Mitchell 1959). Experiments were therefore performed at higher temperatures, and also by rescheduling cooling rates etc. For this purpose special furnaces were designed and fabricated. Before dealing with the heat treatment procedure evolved the constructional details of the furnaces which were fabricated for the purpose will be described. In the range 1200-1400°C a commercial GLOBAR furnace was used. A platinum furnace was fabricated for temperatures up to 1800°C and a molybdenum (vacuum) furnace for temperatures in the range 1800-2200°C. No plans were

possible to be made for temperatures beyond this in view of the non-availability of refractories and other technical difficulties.

2.3.1 GLOBAR furnace

A GLOBAR tubular furnace heated by four silicon carbide heating elements was purchased. The chamber size is 65 mm dia and 500 mm long, and the constant temperature zone is about 150 mm long. The thermal inertia is rather great, so it took about 18 hr to reach a temperature of 1400°C which is the maximum attainable temperature in this furnace. The temperature sensor is a Pt-Pt/10% Rh thermocouple. Temperature is controlled by an on-off controller-cum-indicator. Figure 2.3 shows the GLOBAR furnace along with the control panel and the autotransformer.

2.3.2 Platinum furnace

To perform experiments beyond 1400°C and up to 1800°C a furnace using Pt/20% Rh wire (dia 0.75 mm, length 14 m) as the heating element was designed and fabricated. Since the resistance of this wire (hereafter referred to as Pt) at room temperature is only about 3 ohm it must be preheated using another coaxial furnace so as to attain a higher resistance; this also facilitates a better control of the temperature. A longitudinal sectional view of the complete furnace is shown in Figure 2.4.

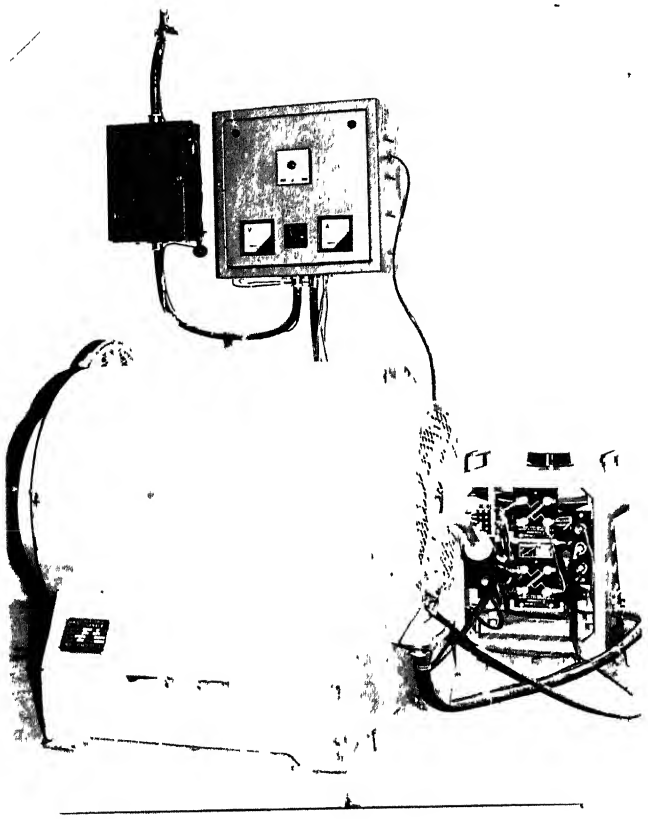

Figure 2.3 GLOBAR Furnace*

*Made by Therelek Furnaces Private Ltd., Bombay

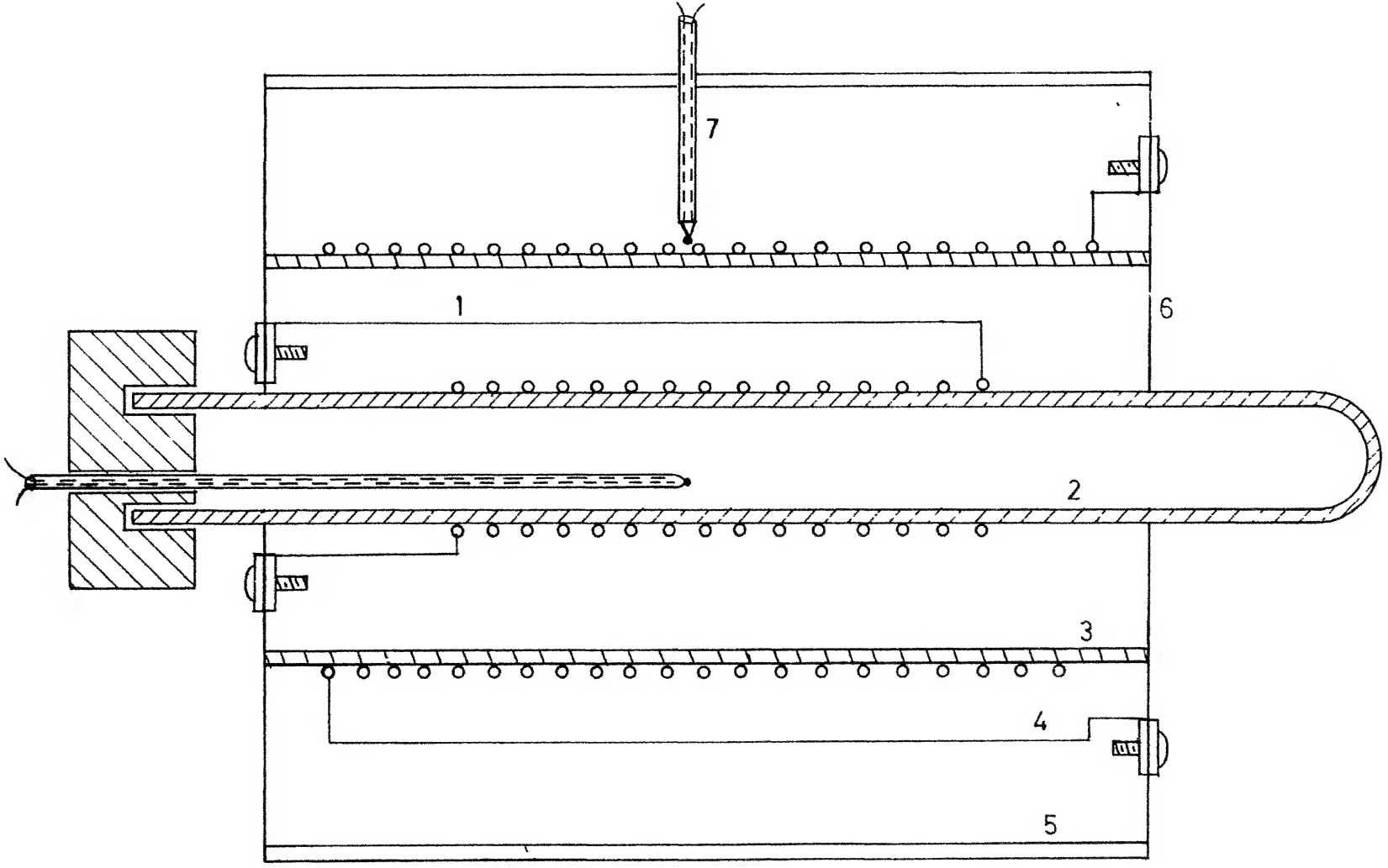

Figure 2.4 Longitudinal-sectional view of the platinum furnace

The platinum wire [1] was wound on a Degussit (West Germany) AL23 tube [2], (dia 50 mm, length 600 mm) over a length of 250 mm in such a manner as to get a uniform heat zone of 100 mm in the middle. A special cement obtained from Carborundum Universal Ltd, India, was applied over the winding and was allowed to set properly. The platinum winding was surrounded by a silimanite muffle [3] (dia 115 mm, length 375 mm). Kanthal wire [4] (dia 0.5 mm, length 10 m) was wound on the silimanite muffle over a length of 350 mm. Fire cement was applied over the Kanthal windings and allowed to set. The diameter of the silimanite muffle was so chosen that its temperature would not exceed 1100°C when the temperature of the platinum furnace was 1800°C. The Kanthal furnace was placed coaxially around the platinum furnace. They were placed inside a coaxial aluminum case [5] which was closed on one side with an asbestos lid [6] having a hole at the centre to let the platinum-wound tube to pass through. The aluminum case was now filled with pure alumina powder completely and then closed with another lid (also of asbestos). The Kanthal and platinum furnaces were energized through separate voltage stabilizers and autotransformers. The temperature of the Kanthal furnace was monitored with an ordinary photoelectric temperature controller and that of the platinum furnace with the help of a Leeds & Northrup 'Electromax' on-off temperature

controller, using Pt-Pt/10% Rh thermocouples [7] as the sensors in both cases. The Kanthal furnace was first switched on and taken to a temperature of about 1000°C. The platinum winding was then at a temperature of about 700°C, at which temperatures its resistance was about 14 ohm. The platinum furnace was switched on at this stage. Due to the large thermal insulation it took a very long time (30 hr) to reach a temperature of 1700°C. As the platinum furnace was heating up, the power in the Kanthal furnace was correspondingly reduced so as to maintain it at a constant temperature of 1000°C and so that the controller did not go on switching 'on' and 'off' frequently. Temperatures in the range of 1500-1800°C were measured with an optical pyrometer. Figure 2.5 is a photograph of the platinum furnace.

2.3.3 Molybdenum furnace

A molybdenum furnace was designed and fabricated for working at temperatures between 1800°C and 2200°C. A longitudinal sectional view of the furnace is shown in Figure 2.6. 40 mil molybdenum wire [1] was wound over a Degussit AL23 tube (2), closed at one end, over a length of 150 mm so as to have a hot zone of 50 mm. Degussit AL23 can withstand up to 1950°C only; but it could be replaced with, for example, Degussit ZR or similar material which can withstand up to 2200°C.

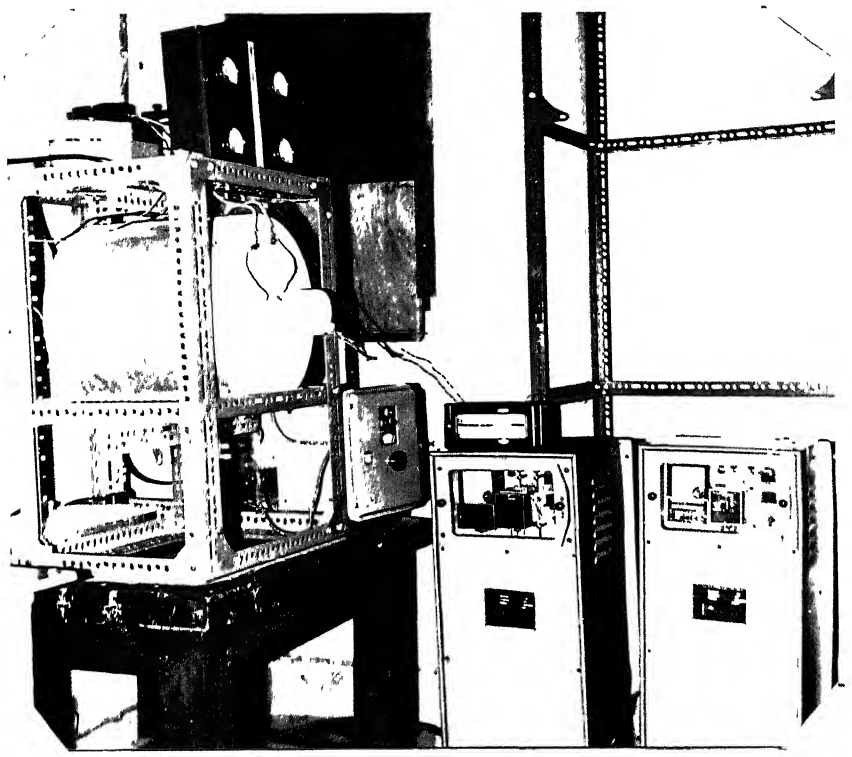

Figure 2.5 Platinum furnace and its control units

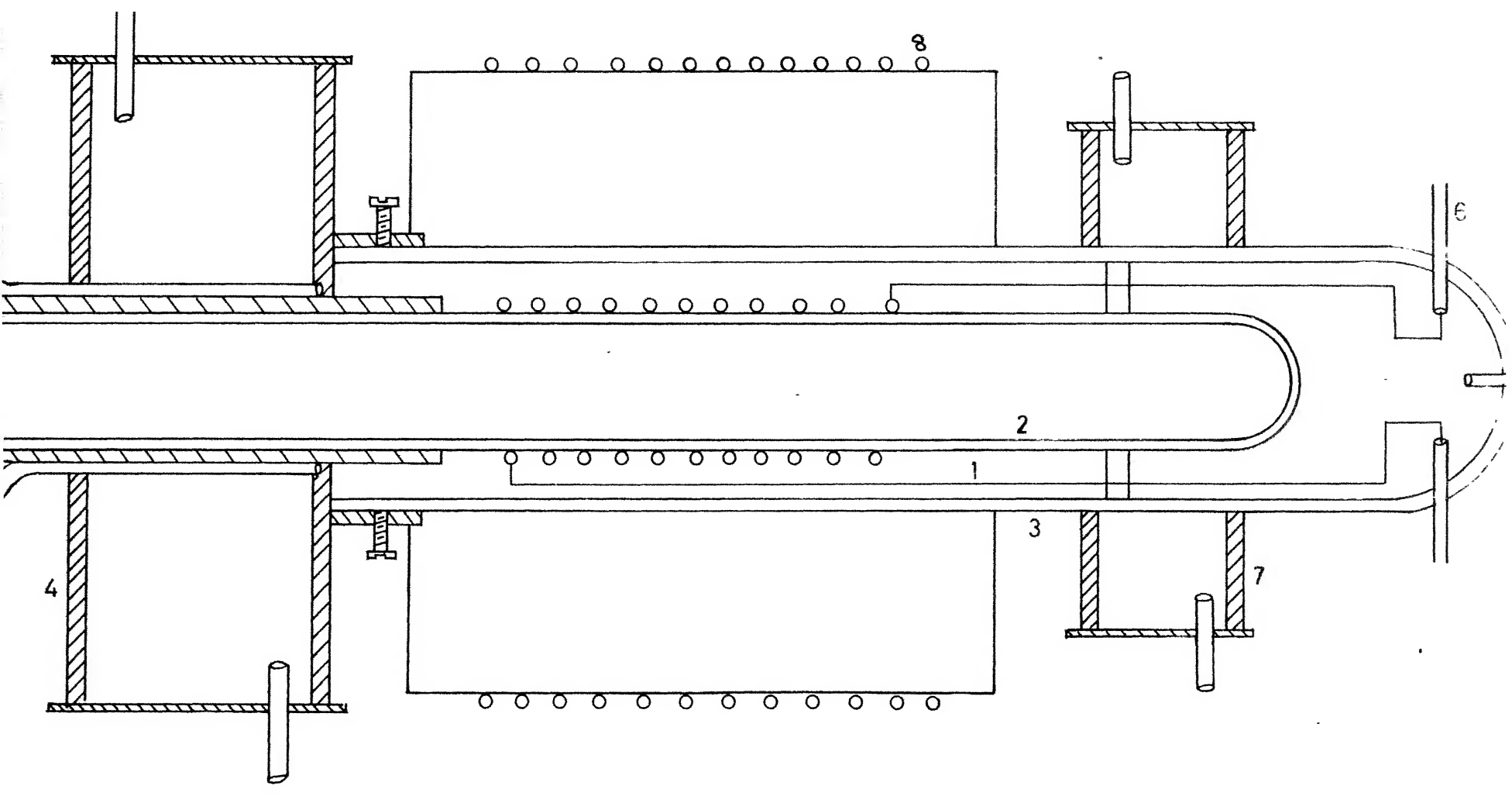

Figure 2.6 Longitudinal-sectional view of the molybdenum furnace

Since molybdenum oxidizes rapidly beyond 300°C it must be held under a reducing atmosphere. So the molybdenum wire-wound tube was inserted inside another close-fitting Degussit tube [3] and provision was made to pass through the interspace hydrogen gas diluted with nitrogen (1:3). For this purpose the open end must be closed but facilities for evacuation and for passing the hydrogen-nitrogen mixture must be provided. Since the temperature near the end would be very high the sealant with which the end might be sealed would soften and thus not keep vacuum. In order to prevent this, the end was closed with a brass water jacket [4] specially designed and fabricated for this purpose. It was, so to say, the 'heart' of the furnace. So every care was taken to ensure that it would not give way during the course of the operation of the furnace. For evacuating and passing the hydrogen-nitrogen mixture stainless steel tubes [5] were fitted through the jacket and brazed with silver solder. The jacket was held to the tube with screws and sealed with a silicone resin (Dow-Corning, USA) all around the joint. The resiliency of the resin is from -65° to 250°C. To take the electrical terminals to the outside and for the gas outlet tube three holes were drilled in the outer tube at the end as seen in the Figure 2.6. The terminals were taken through alumina sleeves [6] which were fixed with the sealant. One water jacket [7] was fitted at this end also to prevent

the softening of the sealant. For measuring the pressure of the gas mixture at the inlet a butylphthalate differential manometer was also made.

This furnace also needs preheating. So the furnace assembly was surrounded by a Kanthal furnace [8] just as was done in the case of the platinum furnace (§ 2.3.2). The entire assembly was mounted on a slotted angle iron frame covered with asbestos sheets on all the sides. Firebricks were placed all around the furnace assembly. A 60 amp, single phase, oil-cooled autotransformer was installed for supplying power to the molybdenum windings. Unfortunately, however, the furnace could not be put into operation due to the non-availability of hydrogen gas. It is hoped to use it for similar experiments later.

2.3.4 Thermal diffusion of Gold

First, two polished and ultrasonically cleaned specimens having {001}- or {110}- faces as the case might be were taken. One specimen was placed in a small platinum box ($5 \times 5 \times 3$ mm^3) and a drop of saturated solution of highly pure Johnson-Matthey gold chloride was put on its upper surface. The other specimen having the same orientation was placed on the first so that a layer of gold chloride solution was sandwiched between the two. The platinum box was closed with a platinum lid. This closed platinum box

containing the sandwich was placed in an alumina crucible (Degussit AL23) which was inserted into the furnace tube. Sometimes a triple sandwich was made. On the two sides of the middle specimen was a layer of gold chloride, in turn covered with another specimen. This was done to see if platinum was by any chance diffusing into the crystals. The later microscopic observations showed that it was not.

The heat treatment consisted in heating to a high temperature, holding the specimens at this temperature for a certain period, and then cooling them in a pre-determined manner. The different parameters involved in the heat treatment are: the holding temperature, the holding time, and the rate of cooling. Of these, programming the cooling rate seemed to be the most important one. A large number of experiments were performed by varying the above parameters. The cooling could be controlled only down to about 400°C below which any of these furnaces cooled down at an extremely slow rate ($<0.5^{\circ}C\ min^{-1}$) even after shutting down the power. But this is not likely to affect the decoration process or anything else. Keeping the holding temperature as 1250°C and the holding time about 48 hr the following cooling rates were tried.

(i) Cooling at the rate of $2^{\circ}C\ min^{-1}$

(ii) Cooling a little faster at $5^{\circ}C\ min^{-1}$

(iii) Cooling rapidly, at about $12^{\circ}C\ min^{-1}$

(iv) Cooling down to 1000°C at the rate of 3°C min^{-1}, aging for 8 hr, cooling down to 800°C, aging again for 8 hr, and then cooling down to 400°C.

With these cooling rates no good decoration was obtained. Then it was decided to increase the holding temperature. The experiments were performed at 1350°C, with the above cooling rates. Still the experiments were not successful. Finally, when the following two-stage cooling rate procedure was adopted the decoration was good, extensive and throughout the crystal. The first cooling was at the rate of either 10°C min^{-1} or 5°C min^{-1} down to 1000°C, and the second at the rate of 2°C min^{-1}. Both Ventron and Semi-Elements crystals showed good decorations when subjected to this heat treatment. However, occasionally there were variations in both. These must be attributed to the original impurity content since all other parameters were unchanged. At times as-received Ventron samples showed crude decoration.

Having established the correct heat treatment procedure for decorating dislocations at temperatures of up to 1300 - 1350°C it was decided to heat-treat specimens at higher holding temperatures. It was anticipated that holding time could be correspondingly reduced. Accordingly the same heat treatment was given, the holding temperature being 1600°C for 15 hr and 20 hr. The decoration was very poor indeed. Experiments performed at 1700°C also did not yield

good decoration. This latter observation is in conformity with that of Miles' (loc cit).

2.4 Observational Techniques

The heat-treated, gold-diffused specimens with {001}-faces were observed as they were taken out of the furnace under bright-field illumination. They were then lightly polished on chamois leather, cleaned with acetone and then with methanol. They were hot-mounted in canada balsam on a glass slide with a cover slip, with the gold-diffused side upward. They were observed under a Reichert RCD dark-field microscope having a maximum magnification of 1250X (under oil-immersion). Most of the observations were made under dark-field illumination. Quantitative measurements on the geometry of the dislocation configurations were made with a calibrated micrometer eyepiece and on photomicrographs. Photographs were taken on a high contrast slow (INDU 10 DIN/8ASA or ORWO 18 DIN/15 ASA) negative emulsion. Exposures were determined by means of Reichert's 'REMIPHOT' vacuum photo-cell exposure meter.

When heat-treated, gold-diffused {110}-section specimens were observed under the dark-field microscope it was found that proper decoration of the dislocations had not taken place. Also gold had diffused only a few microns deep.

Therefore observations were made on {110}-sections prepared from gold-diffused large (3x3x8 mm^3) blocks of the crystal with {001}-faces. Since the specimens were very small they could not be ground and polished mechanically. Therefore they had to be polished chemically. Chemical polishing of magnesium oxide crystals is done by immersing them in boiling orthophosphoric acid diluted with distilled water 4:1 for ten minutes (Stokes 1965).

2.5 Microhardness Measurements

The microhardness of specimens was measured by using a PMT-3 microhardness tester (made in USSR). Microhardness of the as-received crystals, that of crystals heat-treated at 1350°C and subjected to two-stage cooling without diffusing gold, and that of crystals heat-treated and gold-diffused were measured. All these specimens were taken from the same respective stocks of the material (Semi-Elements and Ventron).

Chapter 3

OBSERVATIONS

3.1 Introduction

The observations, mostly by dark-field microscopy, on as-received, undoped heat-treated, and doped heat-treated single crystals of magnesium oxide are presented in this chapter. In order to determine whether impurity precipitates in heat-treated crystals were birefringent polarization microscopy was done; however, not much information could be obtained because the particles are too small. In any case, from the point of view of dislocation configurations duly decorated by the impurity, this information is not very relevant.

Optical microscopy is, on the one hand, relatively simple and direct a method of observation; it is, on the other hand, unable to give information which electron microscopy can. For example, information on the Burgers vectors of various dislocations seen and on the various crystallographic directions which are not in the plane of observation cannot easily be had. Since magnesium oxide cleaves along {100}-

planes* it is easy to recognize <100> and <110> -directions in any cleaved specimen. It was possible to recognize {110} -planes by measuring the angle made by a specific planar configuration with the plane of observation; the refractive index correction was invariably applied. If the angle was 45°, the plane was recognized as {110}. As the specimens into which, as described in the previous chapter, gold chloride had been diffused contained innumerable particles of a second phase, decorating or not, there was the inevitable scattering into the field of view of the dark-field microscope. However, it has been possible to take reasonably good photomicrographs.

As in any other material, decorated or otherwise, observed by optical microscopy or electron microscopy, the kinds of configurations of dislocations are many. The specimens to be described here showed usual dislocation forests, sub-boundaries, etc. In an earlier communication (Parasnis et al 1973) from this laboratory the phenomena observed when specimens had been given a one-stage heat treatment were described. The major conclusions of this earlier work were the following:

---

*Sometimes crystals cleaved along {110} even when the chisel/blade was oriented so as to give the usual {100}-cleavage. The cleaved {110}-surfaces were almost as smooth as cleaved {100}-surfaces. However, such cleavage could not be had at will. It was frequent but accidental.

(i) Dislocations in single crystals of magnesium oxide could be decorated by thermally diffusing gold chloride into the crystals.

(ii) The larger second phase particles (very probably metallic gold) punch out sequences of prismatic dislocations which get decorated during the later stages of the heat-treatment.

(iii) Substantial climb occurs even at temperatures as low as 0.43 T_m.

(iv) Isolated loops of a rather unusual shape were seen.

(v) 'Christmas tree' - and spike-configurations observed by Miles (1965) in as-received crystals were never seen.

The procedures of this earlier work were modified considerably in order to have better decoration so that a multitude of phenomena could be studied. The essential modifications were in the heat-treatment and in the subsequent specimen preparation (see Chapter 2). Among the various phenomena observed the predominant were dislocation dipoles; loops in various orientations; straight-segmented, parallellogram-shaped loops; and combinations of these. It is these which are described, without attention to ordinary sub-boundaries and forests of which there were very few any way.

Dark-field microscopy is often tricky in the sense that objects which are on different planes may be seen in reasonable focus at the same time, giving the impression that they are on the same plane. It has usually been possible in the photomicrographs displayed in this chapter to focus the microscope in such a way that the salient features are brought out at once. Nevertheless it has been necessary to point out that, for example, a certain loop is in fact inclined to the plane of observation (invariably {001}) though in the micrograph it looks entirely in focus. In the case of loops which are parallel to the plane of observation the context and the photomicrographs will make it clear that a loop lies entirely in the (001)-plane.

3.1.1 As-received specimens

Specimens cleaved (and, if necessary, polished) from as-received stock material were examined under the microscopes before subjecting them to heat-treatment. Clearly, they could not for fear of contamination be mounted for observation under the highest magnification. The most that could be done was to observe them under 60 x 12.5 = 750X. As far as dark-field microscopy is concerned this is of no consequence. Semi-Elements specimens very rarely showed any particles within their body. Ventron (99.9% pure)

specimens occasionally showed bright points or strings of bright points. Whether these were due to cavities produced in the act of growing or impurity precipitates was difficult to decide. However, we have the feeling that at least some were the latter. Specimens which showed a large number of such features were rejected. As specimens were to undergo strong heat treatment even the use of immersion oil was avoided. Thus it is possible that at least some specimens of dubious quality found their way to the furnace. This was unavoidable.

3.2 Appearance of the Crystal Surface (Figures 3.1-3.2)

On examining the crystals taken out of the furnace after due heat treatment it was found that, although both surfaces had been well polished before, they had become very rugged and that there were heavy deposits on the surface here and there. Figure 3.1 shows rather artistic flower-like shapes of deposits, occasionally complete with stems. At other places on the same specimen could be seen (Figure 3.2) clusters of crystallites in the form of rods about 5-10 μm long. Often there were crystallites in the form of platelets (size ∿15 μm) similarly dispersed over the surface. Appendix A includes some photomicrographs and a brief description of these platelets. If the specimen was mounted (in Canada balsam) the crystallites loosened from the surface

Figure 3.1

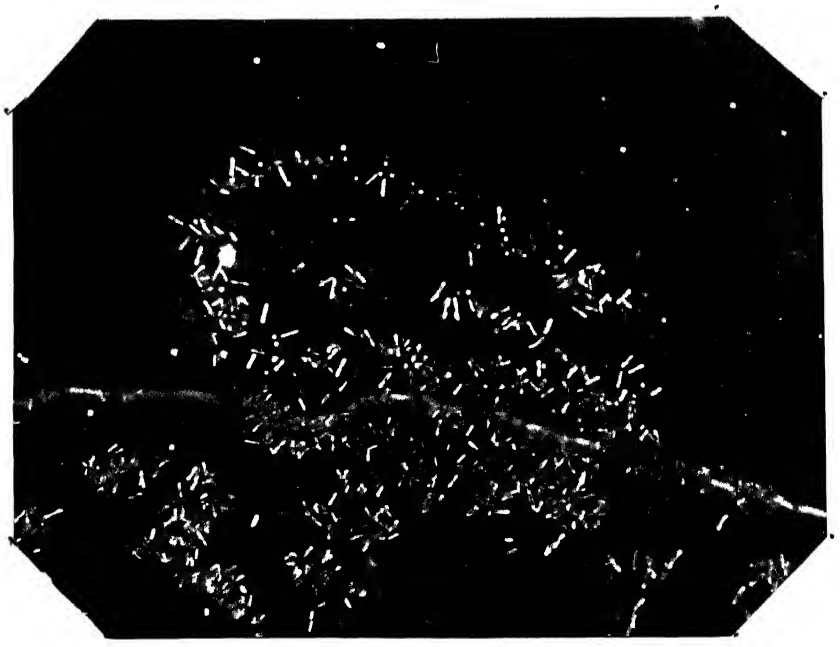

Figure 3.2

and usually floated beyond the specimen edges to be embedded in the balsam away from the specimen itself. These surface features scattered light so much that in order to observe anything within the body of the specimen they had to be removed by light grinding and subsequent polishing as stated in Chapter 2.

No serious attempt has been made so far to determine the exact nature of these material of crystallites. It would be interesting to do so though, clearly, the deposits are likely to be some complex of gold chloride with moisture, already existing impurities and/or magnesium oxide. It is proposed to determine its chemical nature in the near future.

3.3 Decoration (Figures 3.3-3.4)

3.3.1 When repolished specimens were (mounted in canada balsam and) observed under bright-field illumination no second phase particles, random or decorating dislocations, were seen. Only under dark-field illumination could the extensive decoration be seen if there was any. Decoration took place throughout the volume in the case of {001}-sections whereas in the case of {110}-sections it took place only to a depth of 8-10 μm, indicating that gold (or gold chloride) diffuses through {110}-surfaces neither rapidly nor considerably. Therefore all observations have been made on {001}-sections. On the other hand, {001}-

surfaces allow easy and considerable diffusion of it. Figure 3.3 shows the general view under a magnification of 230× and Figure 3.4 under 935×. It is seen that the two-stage heat treatment has resulted in the diffused impurity precipitating preferentially in dislocations rather than at random points. Further, as many photomicrographs show (for example Figure 3.10) the decoration is reasonably fine so that it has been possible to study dipoles and loops less than a micron wide.

3.3.2 It was mentioned in Chapter 2 that crystals were heat-treated in various ways, the parameters being holding temperature, holding time, rate of cooling in the first stage, end temperature of the first stage, rate of cooling in the second stage, *etc*. One-stage cooling mentioned in Parasnis *et al* (1973) also was repeated. On the whole, one-stage cooling tended to give usual forests of dislocations, relatively poorly decorated; that, in fact, was the reason for resorting to a two-stage cooling procedure. Among several variations of these parameters two were found to be useful not only from the point of view of good decoration but also of new interesting phenomena. In both of these procedures the holding temperature was 1350°C or so and the end temperature after the first stage of cooling was about 1000°C. The cooling rate from 1000°C to room temperature was $2^{\circ}C\ min^{-1}$ in both cases. The essential

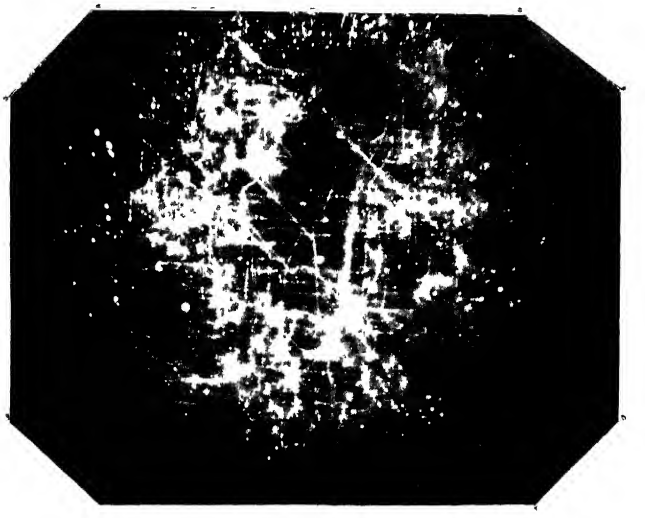

Figure 3.3

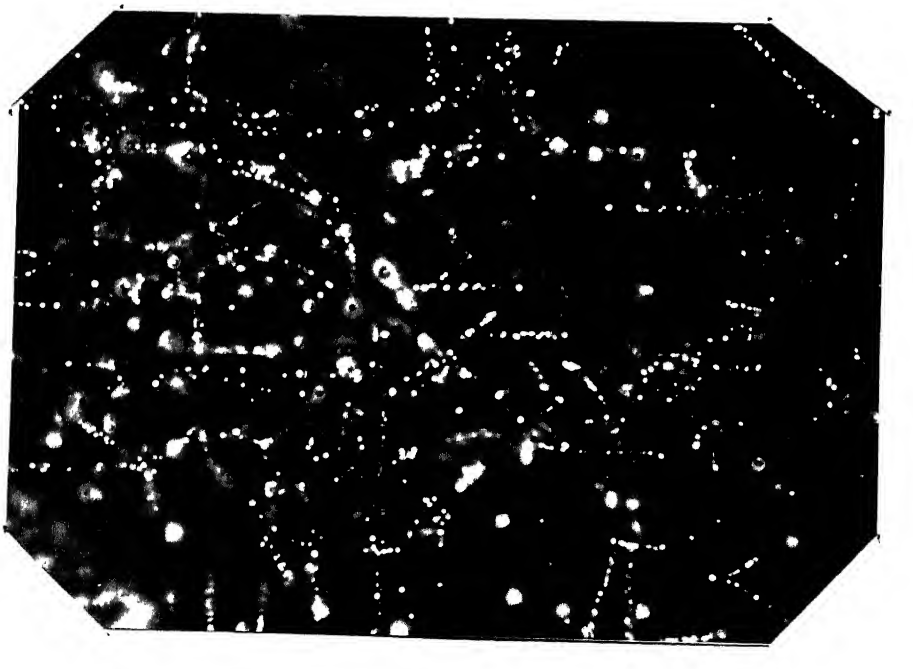

Figure 3.4

difference was in the cooling rate in the first stage, being $10^{\circ}C\ min^{-1}$ in one and $5^{\circ}C\ min^{-1}$ in the other procedure. The results obtained in the two cases are substantially different and are described in detail in §§3.5 and 3.6 respectively.

3.3.3 The most vexing question, to which Miles' (1965) work gives a sharp edge, is whether gold (chloride) is in fact responsible for the decoration observed and for the phenomena studied. It must be confessed that occasionally, but only occasionally, specimens which had been heat-treated in the standard way but into which gold had not been diffused did show decoration, loops and all, even when the platinum box and alumina crucibles used for them had never been used for gold-diffusion. This would seem to confirm Miles' and Lang and Miles' (1965) conclusion that the decoration was due to the exsolution of existing impurities. We are, however, sceptical of such a conclusion. The evidence of the very low frequency of such decoration in our work is strong enough. Stronger still is the observation that {110}-sections prepared from the same block never showed even reasonably good decoration. If exsolution of existing impurities (ZrO_2, CaO or other) were the basic cause of good decoration, simply the fact of the surfaces of a specimen being {110} rather than {001} should make no difference whatsoever. In other words, the decoration

in {110}-sections should be as good. It never was. The decoration therein was in fact so insignificant that it was difficult to observe it, let alone take photomicrographs. We therefore are inclined to believe that the decoration is due to gold although the role of existing impurities is not denied. The third piece of evidence is mentioned in § 3.4.1 dealing with the coloration of heat-treated crystals, with and without gold.

3.3.4 Photomicrographs

Most observations are limited to (001)-sections. In all of the photomicrographs (including Figures 3.3 and 3.4 of the last section) the origin is imagined to be at the left hand bottom corner; the horizontal edge is [100], the vertical one [010] and the normal out of the paper the [001]. [110] and $[\bar{1}10]$ can then be imagined easily, as also the traces of {110} -planes. Occasionally it will be necessary to refer to the projections of directions of the type <011> and <112> inclined to the plane of observation. It is thought unnecessary to refer to the traces and projections every now and then in the subsequent writing.

3.4.1 Colour of the crystals

MgO is colourless to the naked eye. Heating beyond about 700°C imparts a faint but distinct yellow colour to the regions near the edge (less than 0.5 mm wide). In order to

check whether this is due to iron particles from the cleaving chisel/knife/blade embedding into the edges and later diffusing into the crystal, specimens were cleaned very carefully before placing in the platinum box (§2.3.4). Also, platinum is unlikely to diffuse into the crystal. It must be concluded that the impurities existing in the as-received crystal are responsible for the coloration after oxidizing; clearly oxygen of the air plays a part for otherwise the entire crystal would show colour.

Gold-diffused specimens show a much more marked coloration throughout the body, though the very edges are more intense. This far more intense coloration shows that gold has indeed diffused into the crystal. Interestingly, the middle specimen of three placed in the platinum box together (§2.3.4) is far less intensely coloured than the two between which it is sandwiched. It is not proposed to sort out this apparent contradiction in this report.

Detailed ESR and optical spectroscopic work might prove rewarding for identifying the centres responsible for coloration and the elements involved. This was not undertaken as the present investigation is on dislocations.

3.4.2 Micro-Hardness Measurements

Table 3.1 gives the weighted averaged results of micro-hardness measurements as Vickers numbers in Kg mm^{-2}. The

averaging is over several indentations on specimens specially prepared for the purpose in control experiments. All surfaces are {001}.

Table 3.1

Sl No	Specimen	Vickers number ($Kg\ mm^{-2}$) Semi-Elements	Ventron
1	As-received	702 ± 45	642±42
2	Heat-treated, without gold	863 ± 51	830±21
3	Heat-treated, with gold		
	(i) Middle of a triplet	(693 ± 19)	806±32
	(ii) Side of a triplet/ doublet	821 ± 39	838±75

It is seen that our hardness numbers for as-received specimens are in the higher values of the range mentioned by Brookes and Moxley (1975), viz 538-733 $Kg\ mm^{-2}$. The difference between the hardness numbers of as-received and heat-treated crystals is significantly great, about 25%, to assert that the heat treatment hardens the crystals, both Semi-Elements and Ventron. The possible presence of gold does not seem to make much difference; this, of course, is what may be expected.

3.5 Less Slowly Cooled Specimens (Figures 3.3-3.20)

Figures 3.3 and 3.4 of §3.3.1 above show that the dislocations in relatively rapidly cooled crystals are not smoothly

curved; rather they appear somewhat zigzag. (Figure 3.21 of §3.6 which shows smoothly curved dislocations in more slowly cooled crystals may be compared with these.) Both figures show that whatever features are observed have their lengths in the <110>- as well as <100>-directions.

3.5.1 Long and narrow dislocation loops

It is thought advisable before describing the photomicrographs to give, as an aid to the reader, some idea of the shape of long and narrow loops seen and their crystallography. Table 3.2 lists four kinds of similar loops which lie on either {001}- or {011}. In either case the length of a loop, typically 10-125 μm, is parallel to either <100> or <110>; the width is never greater than about 1.6 μm.

In Figures 3.5(a,b) are seen these various long and narrow loops. The two decorated sides of a very narrow loop lying in the plane of observation can often not be distinguished as separate because the decorating particles are large enough to touch one another and thus obliterate the width. In such cases, as can be seen, the decorating particles appear as short segments across the loop rather than as dots. A loop lying in (010) such as the one at bottom middle of Figure 3.5a, which is seen 'edge on', can be distinguished as such by the dotty appearance of its

Table 3.2

Loop plane	Loop length along	Typical shape	Symbol	Number of possibilities	Density (Cm^{-3})
{001}	<100>	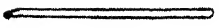	L1a	3×2 = 6	4×10^{7}
	<110>		L1b	3×2 = 6	2×10^{7}
{011}	<100>	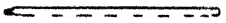	L2a	6×1 = 6	-
	<0$\bar{1}$1>		L2b	6×1 = 6	7×10^{6}
				Total: 24	
{011}	<100>		L3	6×1 = 6	-
{011}	<100>	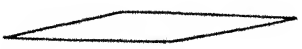	L4	6×1 = 6	-
{011}	<100>	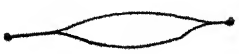	L5	6×1 = 6	-

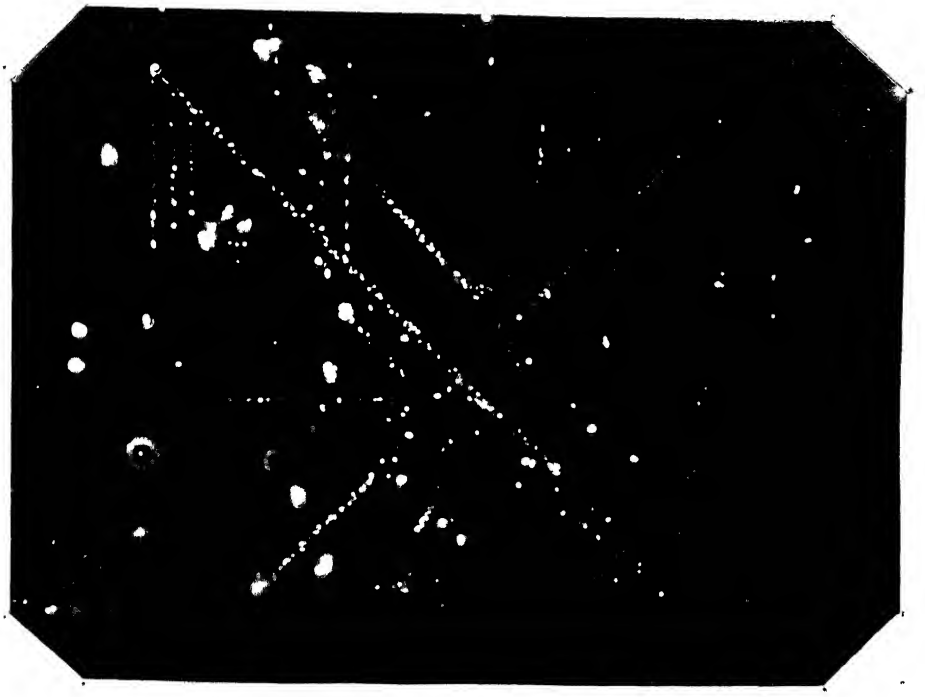

(a)

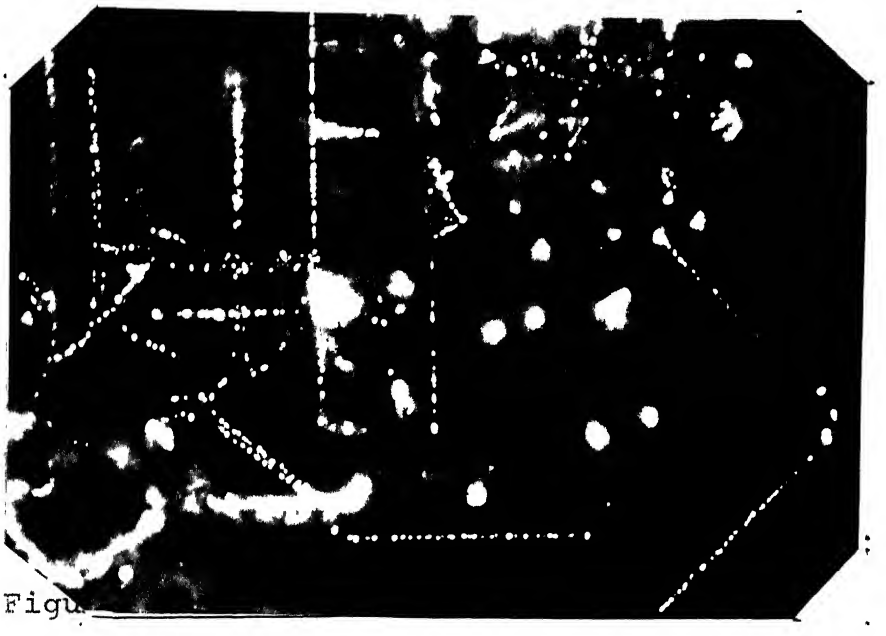

(b)

Figure 3.5

decoration; if the decorating particles are seen as segments at all they lie along the length rather than across. Figures 3.6(a,b) show long loops lying parallel to (001) with their length along [100]. Loops lying in the same planes but with their length parallel to [010] are seen in Figure 3.7; the photomicrograph b of this figure focusses about 4 μm below a. In this figure is seen also a loop, lying along [100] and connected at one end to a cusped dislocation. Other features seen in these six photomicrographs, which among them display eight of the displayable twelve possibilities of Table 3.2, will be described in §3.5.2. Loops which lie in a plane perpendicular to the plane of observation and which have their lengths along the line of sight, viz [001], would show a cross-section of two dots except when the microscope is focussed on either of its ends. It has been possible to follow such loops throughout their length but clearly it is not possible to display them by means of photomicrographs. The cross-sectional dots of a {001}-loop lying along <010> lie along <100> , and those of a {110}-loop lying along <010> lie along $\langle 1\bar{1}0\rangle$. Similarly loops lying in the inclined {110} -planes and having their lengths along $\langle 0\bar{1}1\rangle$ and there are four possibilities- also cannot be usefully photographed. If, however, the length is along <100> , a loop can be photographed. Figures

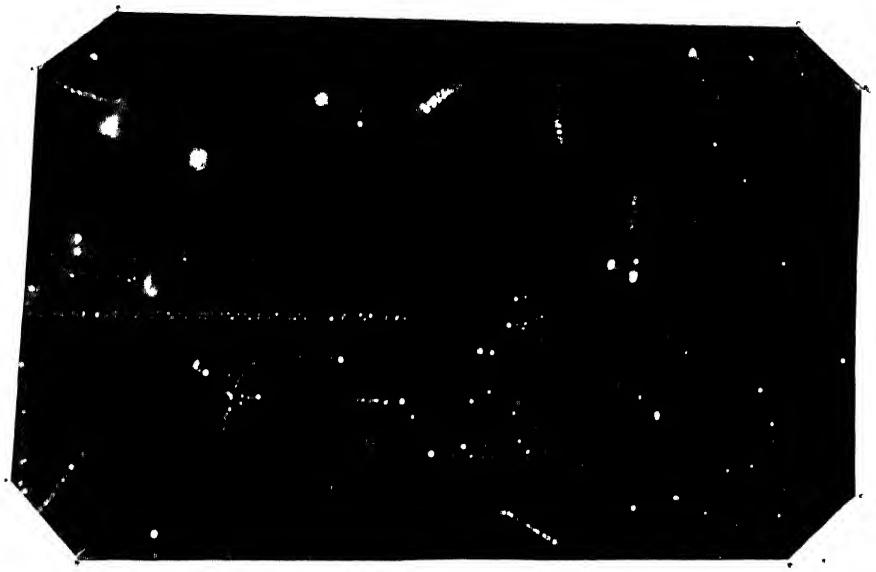

(a)

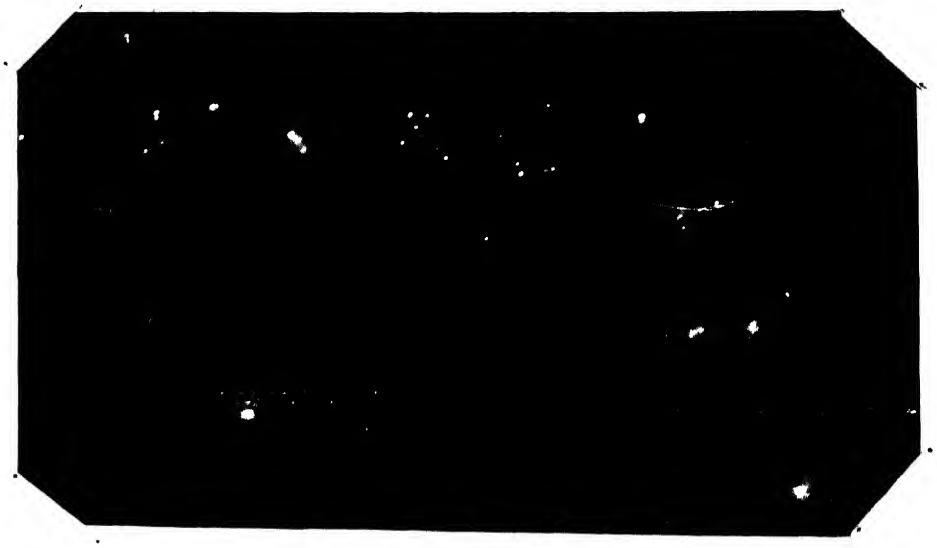

(b)

Figure 3.6

CENTRAL
62236

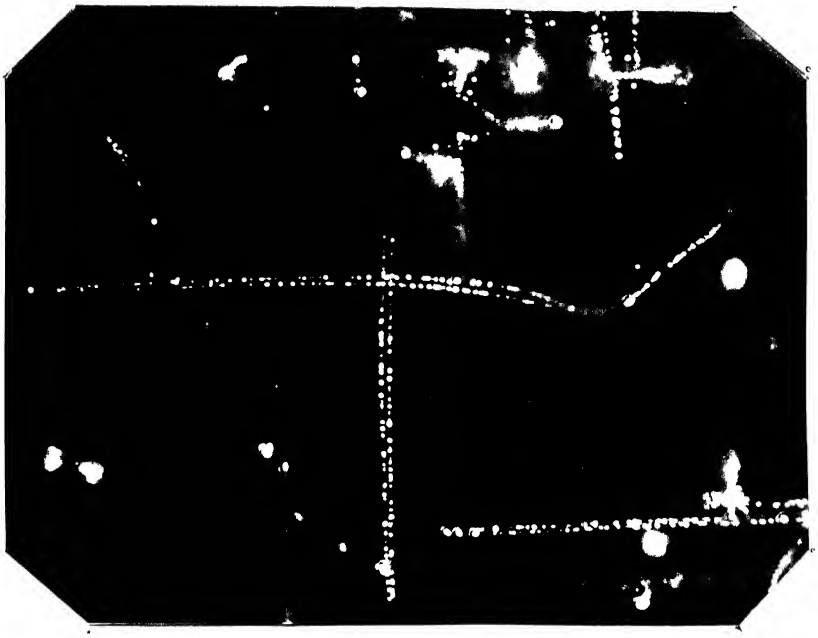

(a)

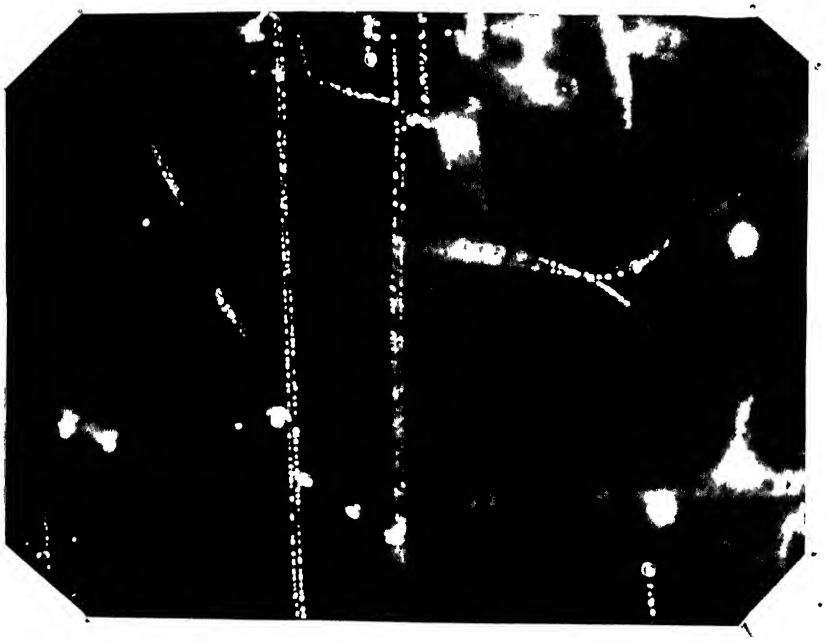

(b)

Figure 3.7

3.8(a,b) show a loop lying in $(01\bar{1})$ with its length along [100]; in a the microscope is focussed on the upper segment only whereas in b it is focussed so as to show both segments, each slightly out of focus. Figures 3.9(a,b,c) show rather unusual loops. The loop of figure a has developed kinks in the middle; the consequent bulge in the middle seems to have straight opposite sides and could be the result of both an interaction with point defects, indigeneous or otherwise, and some stress operating on the loop. The loop of figure b has a bulge of a different character towards one end.

A feature of a good number of loops is that at only one end of each loop is seen a rather large and roughly spherical particle whereas at the other end no such particle is seen. The loop of Figure 3.9c, however, has dots at both ends; it has also a bulge that is unlike that of a or b. Table 3.2 gives the density of loops also. Loops with dots at both ends are less numerous by a factor of 10.

The phenomenon of prismatic punching described in Parasnis et al (1973) is not observed in these relatively rapidly cooled crystals, presumably because large enough particles do not seem to form.

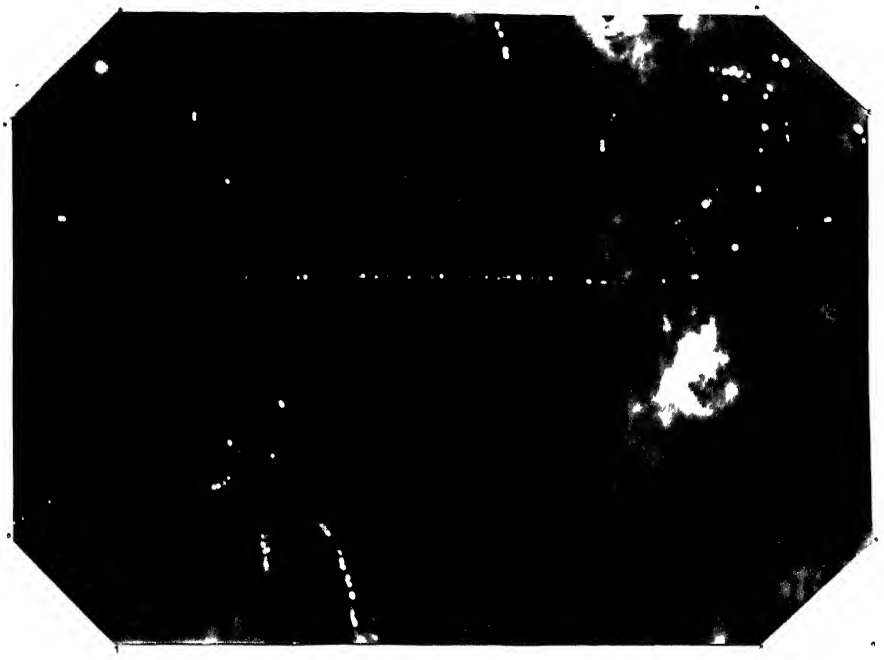

(a)

(b)

Figure 3.8

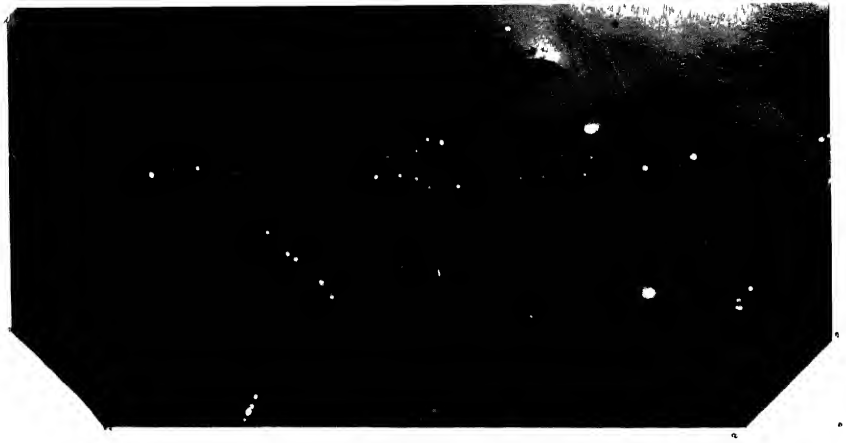

(a)

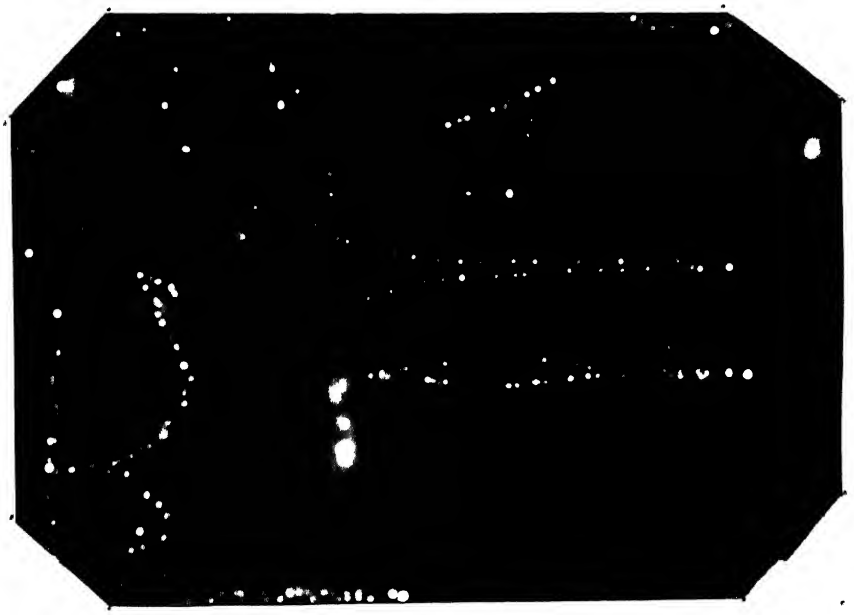

(b)

(c)

Figure 3.9

3.5.2 'Eiffel Towers'

In the foregoing Figures 3.5b, 3.6b and 3.9b are seen dislocations resembling in shape the Eiffel Tower and we shall for brevity describe them by this name. Like the loops described in §3.5.1 the Eiffel Towers have a large and roughly spherical particle at the tip. Figure 3.10 makes it seem likely that the mechanism of formation of both (long and narrow) loops and Eiffel Towers is the same. However, as discussed in Chapter 5, other mechanisms may and do exist. To the left of the main sequence can be seen another, rather faint one, wherein the towers have a very small width. It may be noted that the towers of Figures 3.5b, 3.9b, 3.10 and 3.11 lie in (001) and along <010>.

On the other hand, the tower seen in the middle of Figure 3.6b is in a plane inclined to (001) as indicated by the fact that parts of it are out of focus. More of such can be seen in Figures 3.12(a-e). In all cases the angle made by the plane of the tower (including the legs) with (001), measured in the usual way, was found to be $(45\pm3)^{\circ}$. It is concluded that the plane is nominally {110}; however, it is not concluded that the legs and the tower are in the same plane. The tower seen in Figure 3.12c makes it clear that (i) the two legs are actually in parallel, close-spaced (110)-planes and (ii) the plane of the tower itself

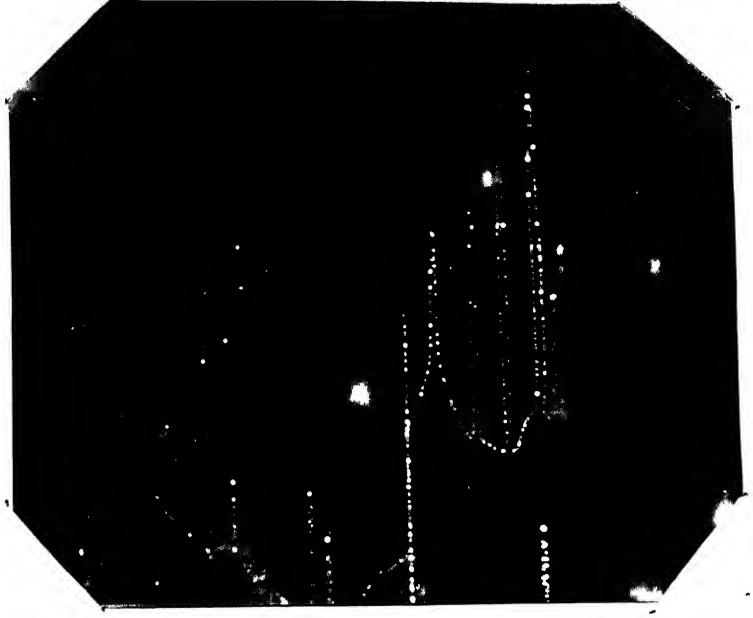

Figure 3.10

Figure 3.11

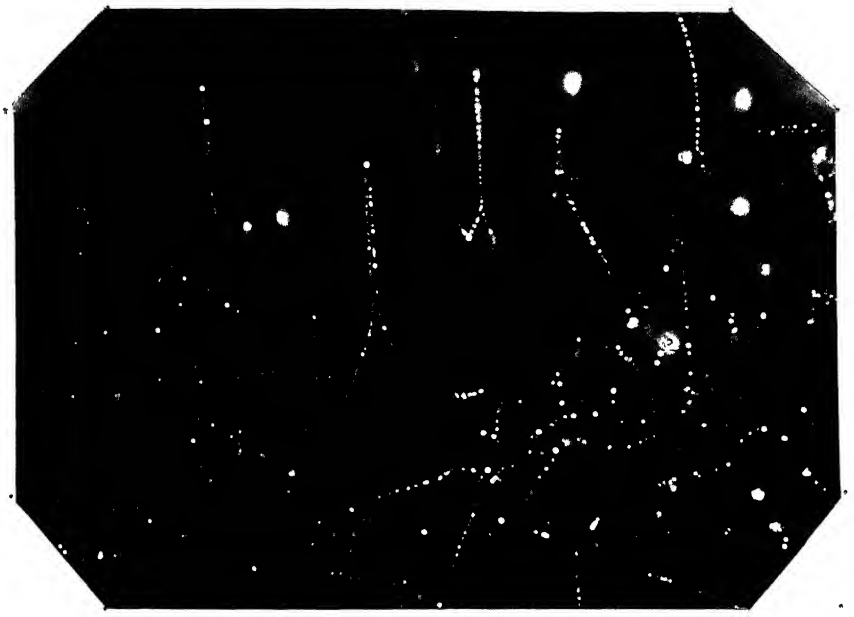

(a)

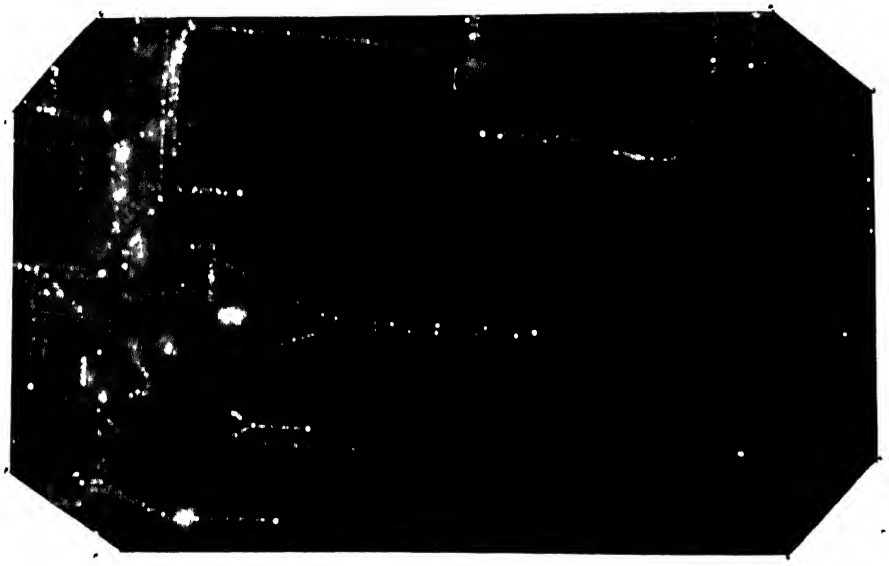

(b)

Figure 3.12

(c)

(d)

(e)

is, in this case, (010). On the other hand, the plane of the upper part of the tower seen in the centre of Figure 3.12a may be (001), $(10\bar{1})$ or (101) in any of which cases the width is clearly seen, unlike Figure 3.12c wherein the upper part of the tower was seen edge-on. In all cases the legs are more or less straight (and this can be seen quite clearly in some of the photographs) in contradistinction to the towers lying on (001) of which the legs are curved considerably (*vide* Figures 3.9b, 3.10 and 3.11). The matter will be discussed in detail later in Chapter 5; suffice is here to inspect the schematic drawings of Figure 3.13. These towers lie in {110} whereas the observation is made in the (001)-plane. Consequently only the angle θ' between the projections of the legs rather than θ can be measured. Table 3.3 gives the results of the measurement and Figure 3.14a is a frequency diagram based on them. It shows that there is a bunching of the values of θ' around about 54°. This is also the angle between <210>-directions which are the projections of the $\langle 1\bar{1}2\rangle$-directions on the (001)-plane. We therefore conclude that the legs of an Eiffel Tower lying in {110} are actually along $\langle 1\bar{1}2\rangle$. This is a rather surprising conclusion in view of the fact that edge dislocations lying in {110}-planes and parallel to $\langle 1\bar{1}2\rangle$-directions are, as elaborated in §1.8, configurationally

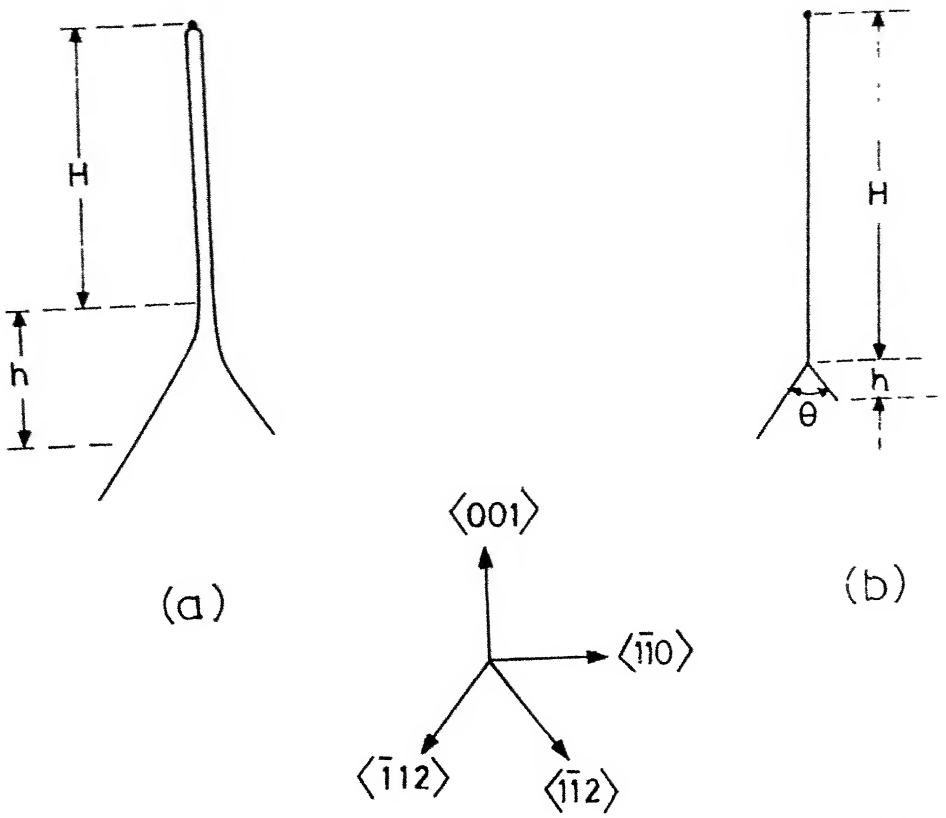

Figure 3.13 The (schematic) appearance of 'Eiffel Towers' in {110}-planes

Table 3.3

Tower No	θ'	Tower No	θ'
1	63°	16	42°
2	62°	17	38°
3	$52^{\circ}45'$	18	49°
4	59°	19	$51^{\circ}40'$
5	50°	20	61°
6	54°	21	50°
7	53°	22	$52^{\circ}10'$
8	$57^{\circ}30'$	23	42°
9	43°	24	$50^{\circ}15'$
10	46°	25	$51^{\circ}35'$
11	$48^{\circ}40'$	26	$55^{\circ}40'$
12	$54^{\circ}10'$	27	$61^{\circ}35'$
13	$48^{\circ}30'$	28	$55^{\circ}20'$
14	$50^{\circ}20'$	29	$63^{\circ}30'$
15	52°	30	$54^{\circ}30'$

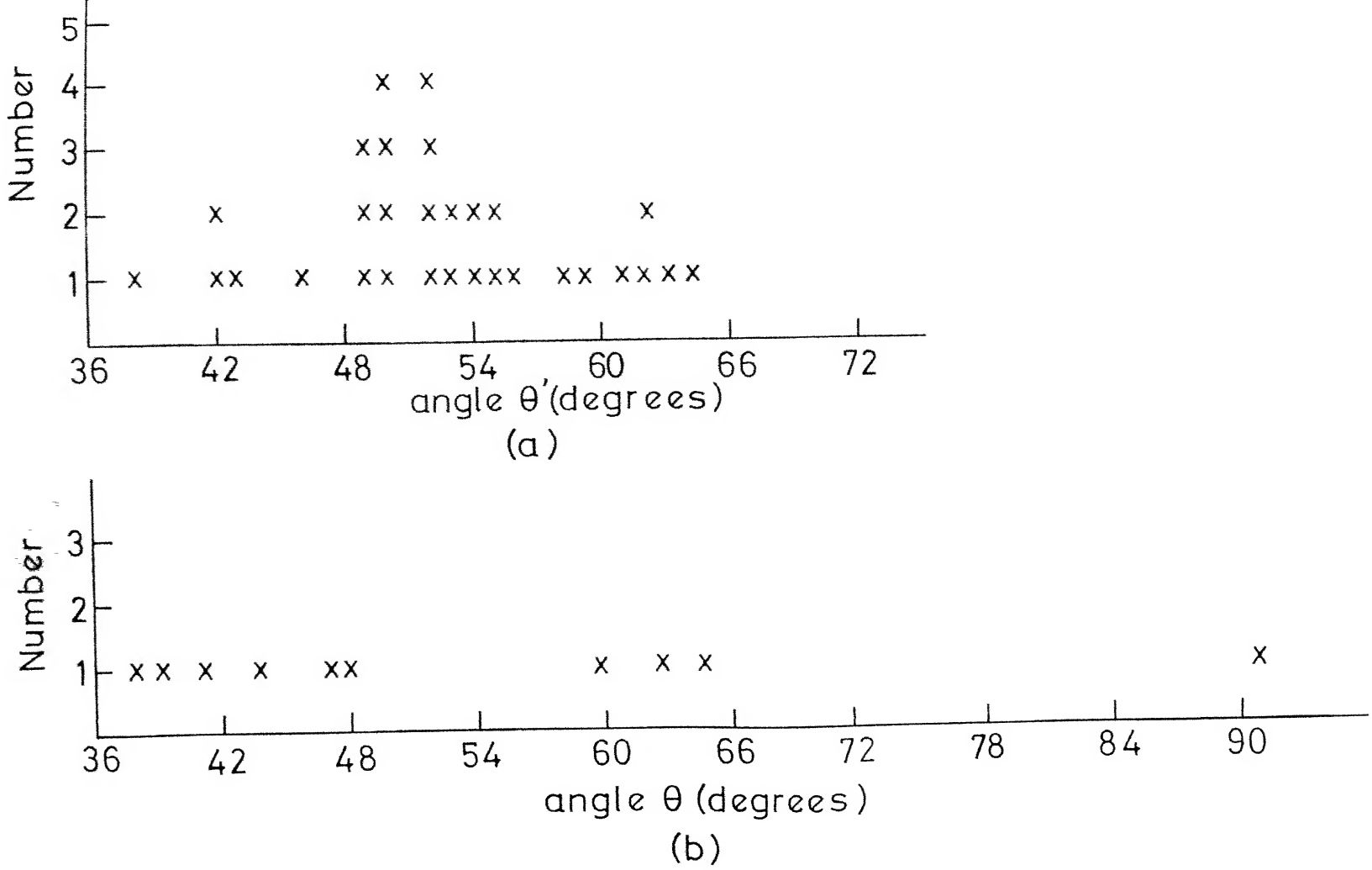

Figure 3.14 Frequency diagrams of (a) the angles between the projections of the legs of {110} towers onto {100} and (b) the angles between the legs of {100} towers.

charged. Figure 3.14b is a frequency diagram of the angle between the legs of those Eiffel towers which lie in (001). Since in this case there is a random spread without bunching we conclude that the legs of {001} - towers are not along any specific crystallographic direction; indeed since the legs are curved, the angle-measurement is not quite justified.

Figure 3.15 shows yet another feature. This is a sequence of spikes, the like of which is also seen in Figure 3.6a. The spikes differ from the towers in {110}-planes in that, first, their forms are not well developed and, second, their sequences lie roughly in {100}-planes. In common with the long loops and the towers there is at the tip of a spike a large particle. The spike sequence of Figure 3.15 actually does not lie in a single plane, (001) or other. Another feature is that the spikes towards the left have almost no base; it develops more and more whereas the height of the tower H decreases almost to nil as one goes towards the right. The same is true of the spike sequence of Figure 3.6a.

3.5.3 Somewhat unusual configurations

In Figures 3.16-3.20 we show some unusual features observed. Not all of these will be discussed in Chapter 5; they are included here as evidence of an extremely wide variety of

Figure 3.15

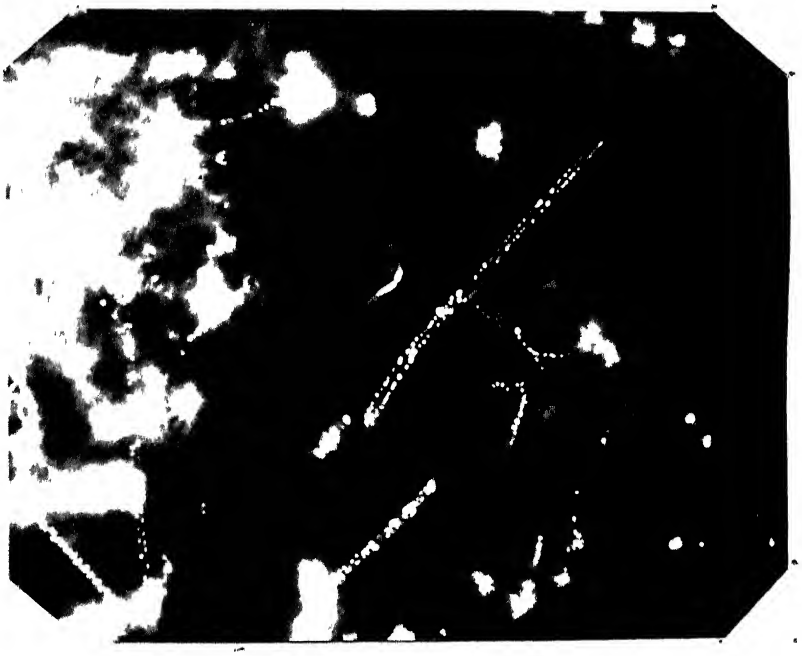

(a)

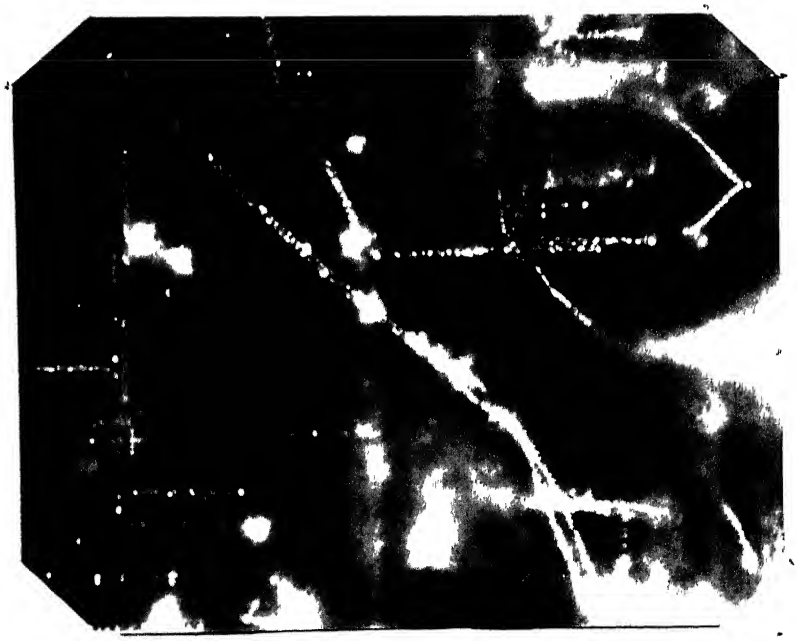

(b)

(a)

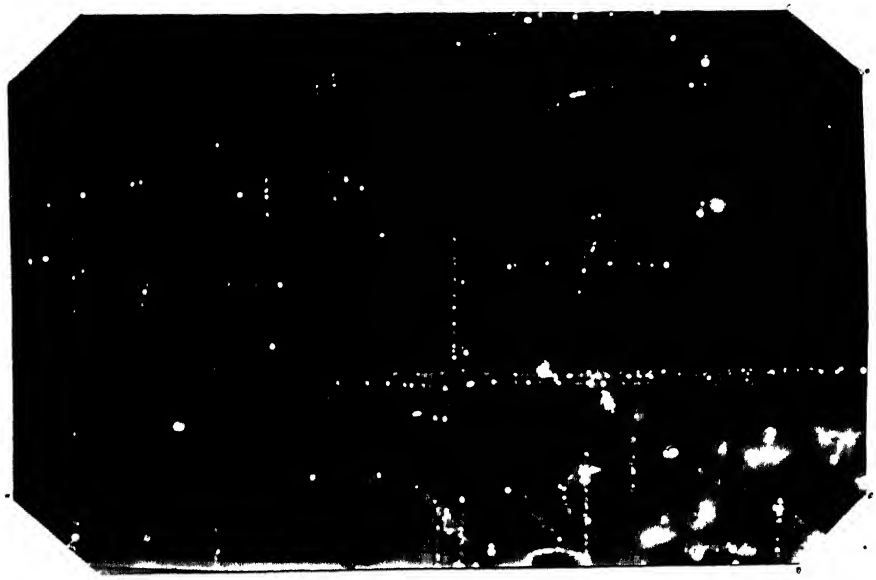

(b)

Figure 3.17

Figure 3.18

(a)

(b)

Figure 3.19

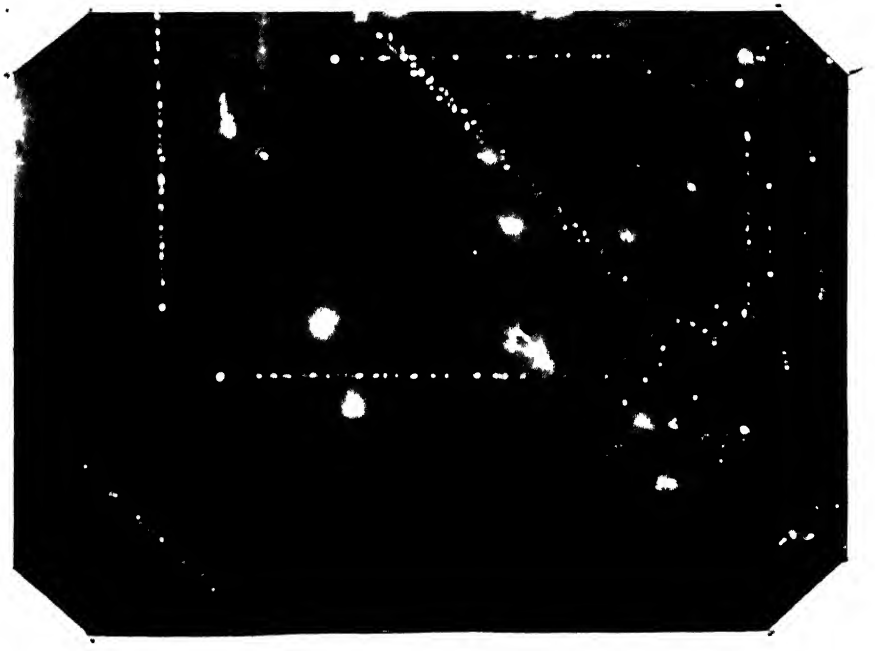

Figure 3.20

dislocation configurations and phenomena occurring in the crystals.

The loops of Figures 3.16(a,b) are unusual in that they have a taper at one end and they have perhaps not been formed completely yet. Figures 3.17(a,b) are extremely unusual configurations in the form of a T-junction and cross-roads respectively. The rather complicated combination of a zigzag loop and a few spikes seen in Figure 3.18 probably has crystallographic significance: the middle inclined segments of this combination make angles of 27° (lower segment) and 34° (upper segment) with $[\bar{1}00]$ which are almost precisely the angles made by <210> and <320> with $[\bar{1}00]$. Since the accuracy of photography and angle measurement is not more than about $\pm 3^{\circ}$ the upper segment appearing to be along <320> is probably fortuitous; it probably is parallel to the lower one and both are parallel to <210>. The sequence seen in Figures 3.19(a,b) consists of almost all the features together: spikes, a somewhat squat tower and loops. (b is about 5 μm below a.) The Eiffel tower seen in Figure 3.20 is puzzling because unlike those of §3.5.2 it is directed along <110> ; also the connection of its legs with other dislocations is not seen very clearly.

3.6 Less Rapidly Cooled Crystals (Figures 3.21-3.27)

Crystals which in the first stage of cooling were cooled less rapidly, viz $5^{\circ}C\ min^{-1}$ against $10^{\circ}C\ min^{-1}$, do not show any of the features described in the last section. However, we do not know if this difference in heat treatment has much significance or there is some other parameter of significance which is as yet unknown. Figure 3.21 shows the typical decoration observed in these crystals. The dislocations go in a smoothly curved sweeping manner; in other words, they do not have an 'angular' appearance. For example, instead of long and narrow loops rather large lenticular loops are seen. Figures 3.22(a,b,c) show a typical loop of this type. The microscope is focussed successively on different parts of the loop, each step being about 4 μm lower. The angle which the plane of the loop makes with (001), measured in the usual way, is about 45° from which we conclude that these loops lie in {110}-planes. As these micrographs show, the loops are cusped along <100>.

In addition to the lenticular loops are observed also parallellogram-shaped loops such as those seen in Figures 3.23(a,b) and 3.24. In Figure 3.23(a) the microscope is focussed on the upper two segments of a loop while in the lower it is focussed midway so as to show the entire loop, of course, slightly defocussed. It has not proved possible

Figure 3.21

(a)

(b)

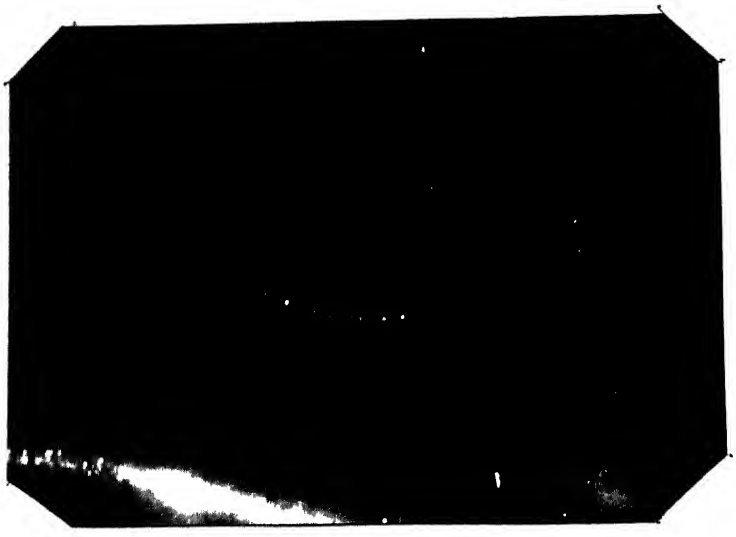

(c)

Figure 3.22

(a)

(b)

Figure 3.23

Figure 3.24

even to make an intelligent guess at the crystallographic directions to which the sides are parallel. Figure 3.24 shows two of these loops lying respectively on (011) and (0$\bar{1}$1). In Figure 3.25 is seen a similar loop the sides of which are slightly rounded and which seems to be connected at one end to another dislocation. As the crystallography of these loops is thus not clear we do not propose to discuss them in detail. They have been displayed here for the sake of completeness.

In Figure 3.26 is seen what is clearly a helix - of two and a half turn - the projection of which on a plane normal to its axis is lenticular like the loop of Figure 3.22. This indicates that the latter is, unlike the loops of § 3.5, prismatic. Helices of this kind were apparently observed by Lang and Miles (1965) by X-ray topography.

The only feature in these crystals which is common with those described in § 3.5 is the spike sequences (Figure 3.27). Notwithstanding the, perhaps insignificant, difference between the two kinds of heat treatment the origin of spikes must be the same in the two.

3.7 Previous Work on Dislocations in MgO

There have been essentially three kinds of investigations on dislocations in MgO.

Figure 3.25

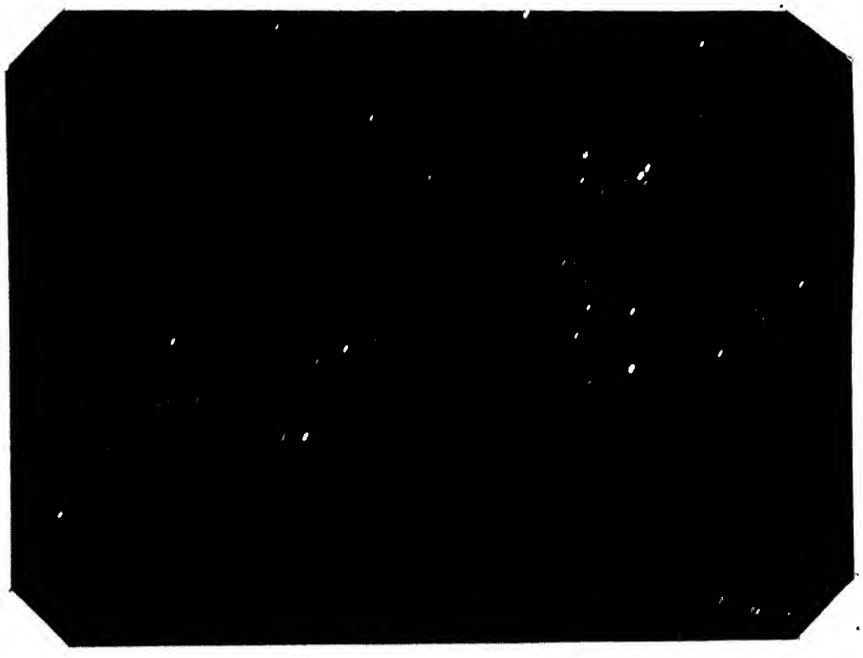

Figure 3.26

Figure 3.27

(i) Study of slip systems, cross-slip, crack formation *etc* by means of etch pits, birefringence and surface markings (Keh 1960, Clarke *et al* 1962, Argon and Orowan 1964(a,b), Day and Stokes 1964, Atkins and Tabor 1967, Fotedar *et al* 1971, Singh and Coble 1974, Brookes *et al* 1975).

(ii) Electron microscopy (Washburn *et al* 1960(a,b); Groves and Kelly 1961, 1962 (erratum), 1962, 1963; Stokes and Li 1964, Washburn and Cass 1966; Narayan 1972, 1973(a,b), 1978(a,b); Narayan and Washburn 1972(a-d), 1973).

(iii) Decoration by existing or intentionally incorporated impurities (Miles 1965, Lang and Miles 1965, Parasnis *et al* 1973).

Quite clearly the present work is of the last kind. When it was begun no electron microscope was available; by the time one became available the work had progressed sufficiently for it not to be abandoned. The work is expected to be continued, using the electron microscope, but for the purposes of this report the work is comparable to that of Miles (1965). The long and narrow loops and the series of spikes observed here resemble the features of Miles' Figures 2, 4, 5. It is necessary therefore to point out the differences between the two investigations. First, the motivation here was quite different (*vide* Chapter 1).

Second, the impurity was incorporated into the crystals intentionally here whereas Miles worked on impurities already existing. Third, as this Chapter has shown, the present work is much more exhaustive even as far as the features common to both are concerned, purely observationally as well as crystallographically. Fourth, in this work many new features have been observed. Finally, here we have attempted (vide Chapter 5) to relate the crystallography of all of the features observed to the formation of dipoles of dislocations; we have also tried to extract new information on dislocations in MgO and on their slip systems. It is indeed planned to extend the work by using an electron microscope (Philips EM 301) and its EDAX system which have become available recently.

Chapter 4

REVIEW OF DISLOCATION DIPOLES AND LOOPS IN SINGLE CRYSTALS OF MAGNESIUM OXIDE

4.1 Introduction

4.1.1 Slip in MgO

Magnesium oxide has the rocksalt structure. It deforms most easily on {110}. The operating slip system at room temperature is $\{110\}\langle 1\bar{1}0 \rangle$ while at high temperatures the $\{100\}\langle 1\bar{1}0\rangle$ -slip system becomes active. Considering the primary slip system viz $\{110\}\langle 1\bar{1}0\rangle$, there are six $\{110\}$ -planes each containing only one slip direction. An edge dislocation lies along <100>-direction while a screw dislocation lies along $\langle 1\bar{1}0\rangle$-direction. An edge dislocation glides in the $\langle 1\bar{1}0\rangle$-direction which is the direction of atomic displacements. Looking at a screw dislocation, atomic displacements in the $\langle 1\bar{1}0\rangle$-direction result in the movement of the dislocation in the <001>-direction. Plastic deformation introduces damage in the form of edge dislocation dipoles and elongated loops. This is due to the frequent cross-slipping of the screw dislocations from {110}-planes on to {010} -planes. The crystals contain dislocations introduced by cleaving and handling in addition

to the grown-in dislocations. The grown-in dislocations are almost immobile as they possess either wrong Burgers vectors or wrong slip planes (Langdon and Pask 1970). So dislocations introduced freshly alone participate in the formation of different configurations. It is thought worthwhile briefly to review the models proposed so far to explain the formation of dislocation dipoles and loops.

4.1.2 Suitability of MgO for dislocation studies

Magnesium oxide is a material particularly suited for a variety of studies on dislocations. Since it is transparent the decoration and birefringence techniques can be used easily. Etching solutions for revealing dislocation sites are simple. Thinning for electron microscopy and x-ray topography can be done simply and reliably by using hot orthophosphoric acid or, better still, by means of an argon ion beam machine. Most techniques of observing dislocations directly are able to distinguish grown-in, fresh and aged dislocations. The melting point is suitably high, 2800°C; this high melting point is, on the other hand, a disadvantage because it is very difficult if not impossible to grow crystals oneself. The really great disadvantage is that the purity of commercial crystals, even those claimed as being 99.9% pure, is suspect. Magnesium oxide is chemically highly stable and not hygroscopic like the

alkali halides; nor is it soft like the silver and thallium halides. Finally, its very simple structure is not a small advantage when it comes to analysing dislocations.

4.2 Mechanisms of Formation of Dislocation Loops in MgO

Almost all the loops observed so far in single crystals of magnesium oxide have been found to have formed from by either the aggregation of point defects or the termination of dislocation dipoles. These mechanisms are described below.

4.2.1 Aggregation of point defects mechanism

When a crystal is heated to a high temperature and cooled, cooling produces a supersaturation of point defects. Consider a supersaturation of vacancies clustering in the shape of a disc on (100)-plane. When this disc of vacancies collapses, a prismatic dislocation loop with Burgers vector a[100] results. This configuration is unstable as it introduces a very high stacking fault energy. In order to eliminate the stacking fault the atoms undergo a displacement of (a/2)[010] on this plane which results in a prismatic dislocation loop with Burgers vector (a/2)[011] (Amelinckx 1964). But recently Zakharov et al (1975) and Narayan (1978a) have

observed prismatic dislocation loops with a<100> Burgers vector (see §4.3 for further discussion).

4.2.2 Dislocation dipole mechanism

This consists of two stages. In the first stage, a dislocation dipole is formed and in the next stage the dipole is pinched off. Various types of interactions giving rise to dislocation dipoles and to their termination have been proposed. Two dislocations lying on neighbouring slip planes and having such configurations as to move towards each other under the action of the same stress create, on coming nearer, either a row of point defects if their slip planes are adjacent, or pass over without interfering if they are far apart. If the separation is of the order of a critical value h given by

$$h \leq \frac{Gb}{8\pi(1-\nu)\tau}$$

where G is the shear modulus, b the Burgers vector, τ the applied stress and ν Poisson's ratio, their mutual stress fields prevent them from crossing over and thus they are said to constitute a dislocation dipole. Elkington et al (1963) found that the separation of the dislocation dipoles in cold worked samples never exceeded the theoretical value obtained from the above expression (about 250 Å).

Koehler (1952) and Orowan (1954) proposed a mechanism on the basis of multiple cross-glide. When a segment of a screw dislocation gliding on {110}-plane cross-slips on to {001}-plane a pair of jogs in edge orientation connected by the cross-slipped screw segment is created. The screw segments continue to glide dragging a pair of edge dislocation dipoles (Figure 4.1a). Johnston and Gilman (1960) suggested a mechanism slightly different from the above, involving a single jog in a gliding screw dislocation. If the jog is equal to one interplanar separation a row of vacancies is created as the screw dislocation glides. In the case of a long jog the two segments glide independently. When the jog is of intermediate height the two edge segments created by the gliding screw dislocation are subjected to their mutual stress fields which keeps them stable and prevents them from crossing over one another and a dipole is created (Figure 4.1b).

Tetelman (1962) considered that the cross-slip of a screw dislocation during the initial stages of deformation is improbable. Electron microscopic investigations have revealed that screw dislocations with tail-like dipoles on both sides are formed. He considered that dipoles are created due to collision mechanism in which two dislocations

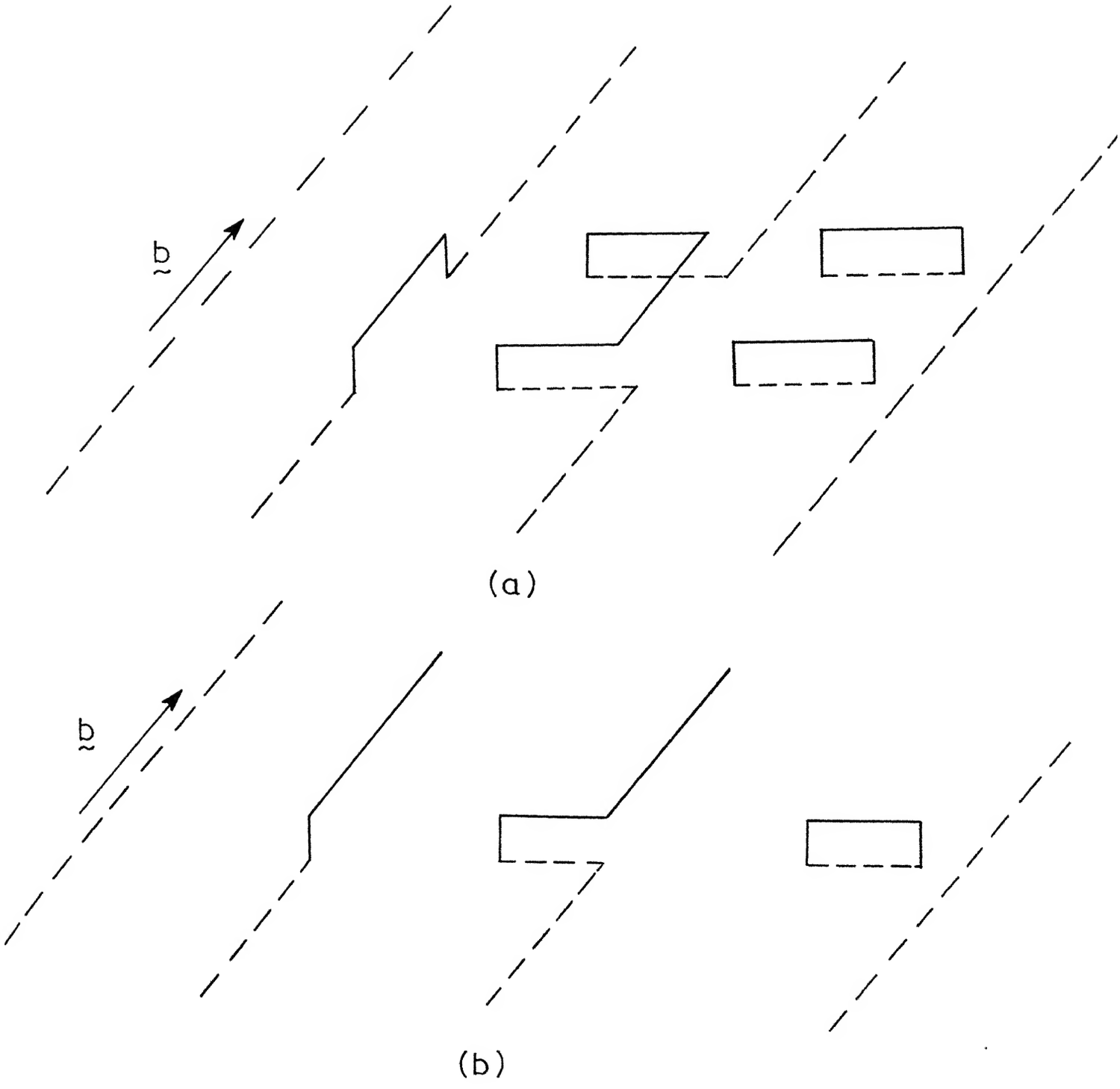

Figure 4.1 (a) Koehler-Orowan mechanism of multiple cross-glide of a gliding screw dislocation resulting in elongated prismatic dislocation loop. (b) Johnston-Gilman mechanism of the formation of a prismatic dislocation loop by the double cross-slip of a gliding screw dislocation. In both a and b the dashed line indicates that the segment is in a parallel plane below the plane of the segment shown by unbroken line.

with opposite Burgers vectors gliding on two neighbouring glide planes, on approaching nearer, orient in such a way that one is directly above the another with edge orientation so as to lower their energy. The screw segment which is already present in one of them or created by kinking cross-slips, resulting in a dipole and a jogged dislocation (Figure 4.2)*. Stokes and Olsen (1963) proposed a mechanism by which a dipole having a length smaller than its height is formed when two screw dislocations with the same sign gliding on the same slip plane cross-link to create a dislocation dipole at the cross-over point.

When a dipole is terminated or pinched off a dislocation loop is formed. Termination occurs by climb at high temperatures whereat vacancies can migrate towards the dislocation core making it climb. Tetelman suggested two ways in which termination takes place by cross slip (Figure 4.3): (1) One of the edge dislocations of the dipole develops a kink (having a screw character) which cross slips and terminates the dipole. This process of kinking followed by cross slip is energetically favourable only when the angle between the dipole and its Burgers

---

*It is customary in the literature to say "...dislocations having opposite Burgers vectors...". This leads to an inconsistency in the diagram of the dipole. We have therefore modified this statement in the text. A reference to Figure 4.2c will show how the 'consistency problem' is solved.

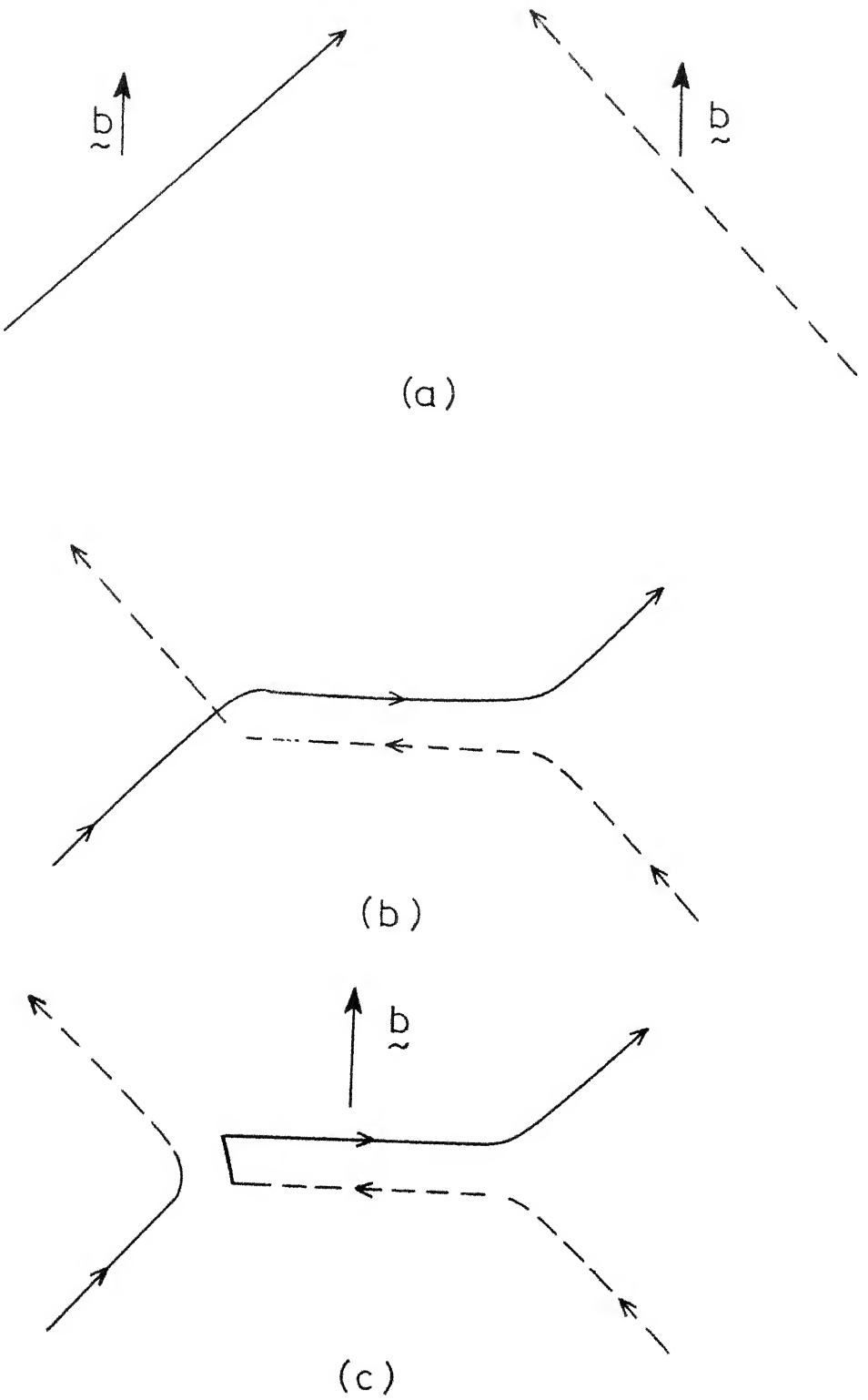

Figure 4.2 Yetelman's mechanism of the dislocation dipole formation (a) Two dislocations with such configuration lying in nearby slip planes gliding towards each other. (b) The edge segments in them reorient so that one is just above another. (c) Formation of a dipole and a jogged dislocation.

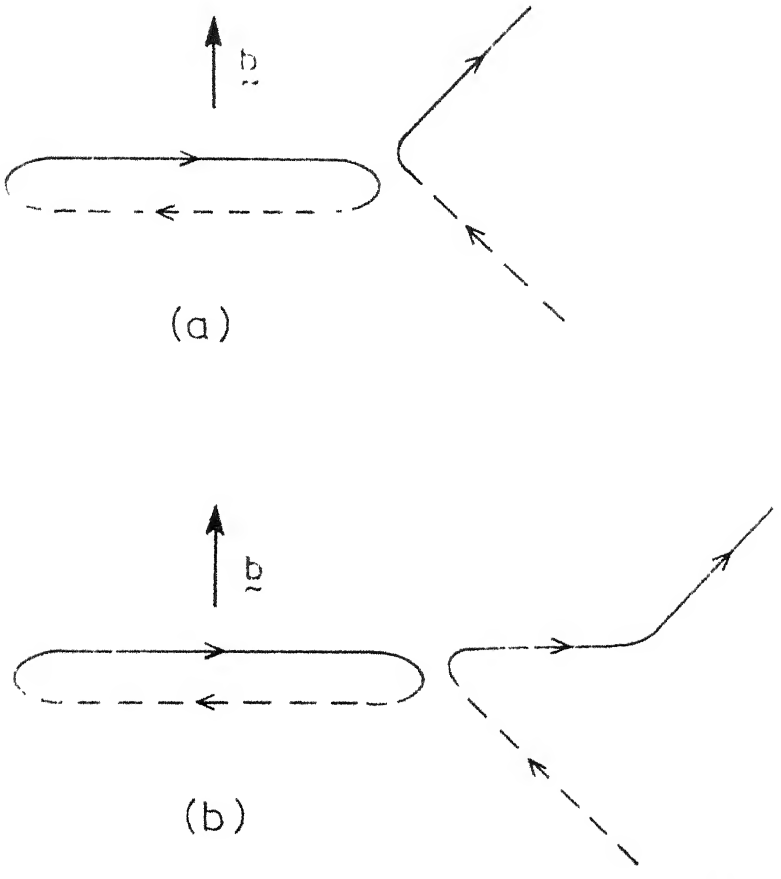

Figure 4.3 (a) Termination of the dislocation dipole by cross-slip at the end. (b) Termination of the dislocation dipole when the component dislocations are of unequal length (Tetelman)

vector is $< 50^{\circ}$. (2) When the arms of the dipole are unequal in length, which is usually the case, termination occurs by cross-slip at the end. But this process needs the help of external stress in the cross-slip plane.

Washburn has suggested that since the unpinned parts of a dipole are usually of different lengths they expand unequally under the action of an applied stress causing the dipole ends to become curved. The configuration in this situation is shown in Fig. 4.4. The two arms of the dipole consist of screw and mixed dislocation segments at the end. The force of attraction between the screw and mixed segments causes the screw segment to cross-slip and terminate the dipole (Washburn 1963). Narayan (1972) obtained evidence for the operation of this mechanism in single crystals of MgO. The terminated end in this case will be slightly bent. Li and Swann (1964) critically analyzed the termination mechanisms due to Tetelman and Washburn and found from their calculations that Washburn's mechanism is the most probable one as it needs least stress for the termination of the dipole. Fourie and Wilsdorf (1960) have pointed out that it is not clear why screw dislocations should suddenly cross-slip in the spectacular manner that is required by either the Koehler-Orowan or Johnston-Gilman mechanism or any of their variants. They suggested that a gliding screw

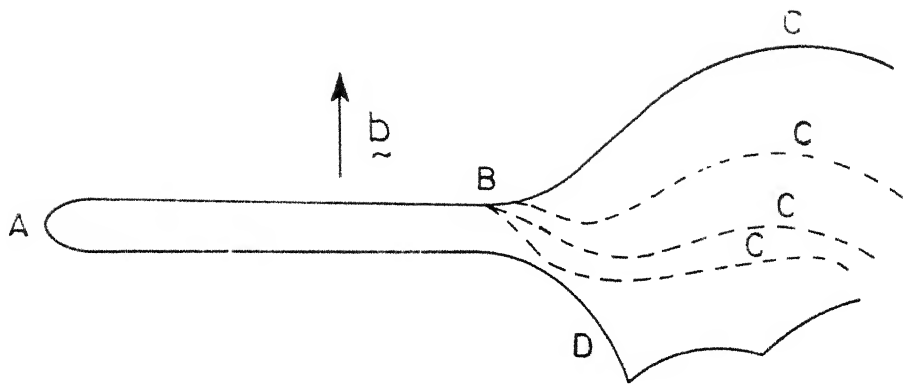

Figure 4.4 Termination of dislocation dipole (Weinburg 1963). AB is the dipole. BC and BD are the screw and mixed segments.

dislocation would form a dipole on meeting a void and that the edge segments of the dipole would climb in opposite directions as a result of the vacancies from the void diffusing to their cores. Pinching of the dipole takes place eventually and an elongated loop is produced that is not a prismatic one; rather, it is a slip-cum-prismatic loop. It is shown in Chapter 5 that some of the loops are geometrically similar to those formed in this, Fourie-Wilsdorf, way.

Termination of a dislocation dipole results in a narrow elongated loop. The width of the loop is about 50 Å. But on annealing these elongated loops break up into strings of circular prismatic loops. The separation between the circular loops and their diameter indicate that the area of the loop remains constant during break up. Groves and Kelly (1962) observed such breaking up of loops in MgO while Price (1960) observed similar breaking up in Zn and Cd. Groves and Kelly developed a theory for the kinetics of the breaking up process with the assumptions that the lattice is frozen outside the dislocation core along which ions are transported by vacancy migration, and that the process is controlled by the movement of ions from one part of the dislocation to the other.

4.3 Dislocation Configurations Observed in MgO

Washburn *et al* (1960) observed for the first time dislocations and dislocation reactions in thin foils of single crystals of MgO using transmission electron microscopy. They obtained direct evidence for the double cross-slip of screw dislocations from {101}-planes on to {010}-planes and back to parallel {101}-planes and dislocations undergoing reactions of the type

$$(a/2)[011] + (a/2)[10\bar{1}] \rightarrow (a/2)[110].$$

Double cross-slip of screw dislocations results in elongated prismatic dislocation loops. Groves and Kelly (1961, 1962a) studied the effect of annealing on plastically deformed crystals. On annealing in the temperature range 1200-1500°C the elongated loops formed during plastic deformation break up into strings of circular prismatic loops (diameter $\sim$500-2000 Å). These loops lie on {110}-planes perpendicular to $\{1\bar{1}0\}$-planes on which slip has occurred and have Burgers vector $(a/2)\langle 1\bar{1}0\rangle$. They correspond to a collapsed disc of vacancies.

Miles (1965) observed in annealed as well as in as-received single crystals unusual decorated dislocation configurations such as christmas trees, spikes, irregular loops *etc*, and regular configurations like long elongated loops and helices. Those observations were made under optical

microscope. The unusual configuration of the 'christmas tree' had greatest projected height of about 50 μm. X-ray topographic studies by Lang and Miles (1965) revealed that the loops whose long axis lies along [100] have Burgers vector parallel to [011] or [0$\bar{1}$1]. The mean direction of the axes of the helices is found to be that of the Burgers vector of the helix, which is [0$\bar{1}$1] for most of them, but with a scatter of $\pm 20^{\circ}$ from the direction of Burgers vector. The distorted helices have the major diameters in the range of 50-200 μm. They concluded that the unusual configurations are nothing but a perturbation of already existing dislocation distribution and that climb is responsible for their unusual orientation. These structures are too large to be seen by electron microscopy.

In addition to vacancy loops, interstitial loops were also observed in plastically deformed and subsequently annealed crystals (Narayan and Washburn 1972a). Dislocation loops observed in single crystals of MgO seem to be all prismatic in character. Vacancy loops with Burgers vector (a/2)<110> associated with impurities such as $MgO \cdot Al_2O_3$ spinel have also been observed (Narayan 1973). Quantitative measurements on the self-climb of dislocation loops were made by Narayan and Washburn (1972b).

Ogawa (1966a,b) observed long dipoles (>1 μm) and suggested that such long dipoles could be formed only by a collision mechanism and not by a rearrangement mechanism (also suggested by Tetelman). He obtained evidence for dipoles formed by the rearrangement mechanism also, which (dipoles) were of very short length (≤0.5 μm). Appel et al (1977) studied the motion of screw dislocations and their interaction with point obstacles by performing in situ-deformation experiments on thin foils of MgO in a high voltage electron microscope The loops observed seem to have formed by the Johnston-Gilman mechanism.

Mitchell et al (1977) studied the irradiation damage in the temperature range 300-970°K and observed a large number of dislocation loops which were of perfect interstitial type lying on {110} with Burgers vectors (a/2) $\langle 1\bar{1}0 \rangle$. These studies were carried out by high voltage electron microscopy. Groves and Kelly (1963) studied the effect of neutron damage in MgO irradiated at a temperature less than 473°K. The crystals become intensely coloured. Most of the ions displaced by irradiation return to their normal sites during irradiation itself. On annealing these irradiated crystals, the damage coarsens and circular prismatic loops are formed.

Parasnis et al (1973) observed equilibrium dislocation configurations like prismatically punched out loops which later expanded by climb and elongated loops (elongated along <100>). Zakharov et al (1975) observed square-shaped prismatic dislocation loops lying on {100}. The sides were parallel to <110> and the Burgers vector was normal to the plane of the loop. Narayan (1978) observed a<100>-dislocation loops of circular shape in thin foils of MgO just before electrical breakdown. Both square and circular loops have been identified as being of vacancy type.

Stokes and Li (1964) found that when a prestrained crystal is subjected to heat treatment above 600°C its strength increases. At higher temperatures and with more prolonged heat treatment there is more resistance to the renewed movement of the aged dislocations. Two hours of heat treatment up to 1000°C results in the complete locking of the dislocations. But bend tests indicated that yielding occurs with jerky flow. This shows that dislocations are being unlocked and this is referred to as weak dislocation locking. Above 1000°C dislocations are locked strongly after 2 hr at 1200°C or 30 min at 1500°C or 15 min at 2000°C.

4.4 Summary

The brief survey given above may be summarized as follows:

(i) At room temperatures the operating slip system is $\{110\}\langle 1\bar{1}0\rangle$ whereas at high enough temperatures $\{001\}\langle 1\bar{1}0\rangle$ also operates. Burgers vectors of the type $a\langle 100\rangle$ are observed for sessile loops only (see ix below).

(ii) A survey of the literature shows that only prismatic loops are observed in single crystals of magnesium oxide. Slip loops (ie Burgers vector lying in the plane of the loop) do not seem to have been observed.

(iii) A gliding screw dislocation undergoes double cross-slip giving rise to an elongated loop lying on $\{110\}$-plane perpendicular to the glide plane of the moving screw dislocation (Koehler-Orowan and Johnston-Gilman; Figures 4.1, a and b respectively).

(iv) Two dislocations lying in nearby slip planes and having opposite Burgers vectors moving towards each other orient in such a way that the edge segments are one above another and thus constitute a dislocation dipole. This dipole terminates by developing a kink (having a screw segment) which cross-slips resulting in an elongated prismatic loop (Tetelman; Fig. 4.2).

(v) Dislocation dipoles invariably occur with the component dislocations of unequal lengths. Because of this they expand unequally under the influence of a stress and thus they become curved. The end of the dipole now consists of screw and mixed dislocations which attract each other resulting in the screw component cross-slipping and terminating the dipole (Washburn; Figure 4.4).

(vi) The above termination mechanism (suggested by Washburn) has been found to be the most probable one in magnesium oxide since it needs least activation energy (Li and Swann 1964).

(vii) The elongated prismatic loops break up into strings of circular loops on annealing.

(viii) Circular loops of vacancy type are formed by the collapse of discs of vacancies. They lie on {110}-planes and are associated with impurities.

(ix) Square-shaped a<100>-dislocation loops lying on {100}-planes (Zakharov et al 1975) are associated with the impurities and have been identified as vacancy loops while the circular loops on {100}-planes (Narayan 1978a) are not associated with any impurity.

(x) Grown-in dislocations in commercially pure single crystals cannot be moved, at room T, even under very high stresses. Fresh dislocations injected into the crystal surface are aged at high T resulting in weak locking (due to impurities) above 600°C and in strong locking (due to configurational reasons) above 1200°C. Heating to 1900°C immobilizes all dislocations completely (Stokes and Li 1964).

4.5 Comment on the Term 'Dipole'

The term 'dipole' is used in the literature for a variety of dislocation configurations. We collect here the distinct configurations for ready reference.

(i) Two parallel, opposite ($\underset{\sim}{b}$, $-\underset{\sim}{b}$), edge dislocations on parallel slip planes, at 45° (Nabarro 1967, p 89, Figure 2.10).

(ii) A semiloop of dislocation, the dipole plane being normal to $\underset{\sim}{b}$, so that the two edge segments of the dipole glide on parallel slip planes (Nabarro, p 383, Figure 6.15).

(iii) A semiloop of dislocation lying entirely in its slip plane, longer segments being normal to $\underset{\sim}{b}$ (Nabarro, p 383, Figure 6.14; Friedel 1964, p 242, Figure 9.3b).

(iv) A semiloop (formed, for example, by Fourie-Wilsdorf mechanism), the dipole plane being at angle to $\underset{\sim}{b}$ other than 90° (Nabarro, p 376, Figure 6.11).

(v) A semiloop, similar to (iii) above immediately upon its formation and to (iv) above after climb, the anchoring at the open ends being due to entirely different reasons (This work, Chapter 5, Figures 5.4, 5.8).

Chapter 5

DISCUSSION

5.1 The Approach

Before embarking upon the discussion of the results obtained in this work a few general remarks may be made. Our approach shall be to search for a mechanism or mechanisms for the final dislocation configurations (Chapter 3) to have come about presumably by equilibration under the conditions of heat treatment and in the presence of (intentional and unintentional) impurities. From among the observations made a few have been selected for a detailed discussion on two grounds: first, they seem to be new; second, they are directly related to the motivation with which this work was undertaken. These are the long and narrow loops, Eiffel towers and the role of the deliberate impurity (Au).

It will be apparent later in this chapter that the upper part of the Eiffel towers is a dislocation dipole. In Chapter 4 was given an account of the various mechanisms invoked by earlier workers to explain the formation of dipoles in magnesium oxide. Long and narrow loops and dipoles have been observed by almost everybody who has

done electron microscopy on magnesium oxide. Admittedly the scale of electron microscopy is quite different from that of the present work but the same mechanisms might be expected to apply here. One obvious reason that they do not, is that loops elongated along <110>, which do not seem to have been observed before, cannot be formed as a result of their operation. The general characteristics of the <110>-loops (ie L1b and L2b) are so like those of the <100>-loops (ie L1a and L2a) that even the latter could not be said to have formed by those mechanisms. Our approach therefore will be consistent with the imposition that the same mechanism shall apply to all long and narrow loops described in Chapter 3.

The third part of our approach is the following. Miles (1965) and Lang and Miles (1965) have tried to explain the occurrence of decorated dislocation configurations purely on the basis of the climb of existing configurations in the as-grown crystals although, as they have remarked in their papers, it had not been possible for them to explain all of the features. Apart from the lenticular loops and the corresponding helices and the {100}-spike sequences there are virtually no common features between the two investigations. It is therefore evident that climb alone cannot explain (or explain away) the Eiffel towers as well as the long and narrow loops. These configurations are

observed only in crystals into which gold has been diffused. We therefore reject simple climb as the basic cause giving rise to them.

5.2 Decoration

5.2.1 The chemical formula given on the label of the vial of gold chloride supplied by Johnson-Matthey is $HAuCl_4 \times H_2O$. This compound, which is simply $AuCl_3$ in combination with moisture, would clearly lose its water as soon as the furnace temperature is reached, say, 25-50°C, above room temperature, and be $AuCl_3$. $AuCl_3$ decomposes into AuCl and chlorine gas at about 260°C and AuCl itself is reduced to metallic gold at still higher temperature (Wise 1964). Both chlorides are ionic compounds, the radii of Au^+ and Au^{3+} being 1.37 Å and 0.85 Å respectively. As far as the diffusion into the crystals of magnesium oxide in the furnace is concerned it is the Au^{3+} ion that diffuses through the surface because (i) its radius is much more favourable, and (ii) since the film of auric chloride was sandwiched between two crystals the chlorine cannot have all formed into molecules and escaped; rather, it must still be in ionic form so that the gold also is in the corresponding ionic form. The details of the diffusion of Au^{3+} need not concern us here but clearly sufficient gold diffuses into the crystals very probably by the interstitialcy mechanism. The deep yellow coloration of the

edges and the lighter coloration of the entire crystal are a result of the incorporation of gold.

5.2.2 The next question is whether gold is responsible for decoration. It has been pointed out in § 3.3.1 that gold does not diffuse through {110}-surfaces and that therefore such attempts at decoration failed. If gold had not been responsible for the decoration, that is if the impurities in the as-received crystals were primarily responsible as in Miles' work, these attempts would not have failed. Further, with appropriate identical heat treatment doped crystals invariably had far better decoration than the undoped crystals which latter had any decoration worth mentioning only occasionally. We have no doubt that decoration is by the precipitation of metallic gold on dislocations. No analysis of the impurities in as-received crystals was available from the manufacturers. A few samples showed* the presence of calcium oxide precipitates (in epitaxial orientation), but not of ZrO_2.

When crystals are heated beyond 1400°C no decoration occurs. We presume that the protracted heat treatment at the higher temperatures made the dislocations anneal out more completely.

---

*We are indebted to Professor D J Barber, Department of Physics, University of Essex, Great Britain, for examining these samples in a JEOL-make 100CX analytical microscope.

This is consistent with the observations of Miles (loc cit) and Stokes and Li (1964).

It has not been found possible to give an explanation of why gold does not diffuse through {110}-surfaces. If the mechanism of diffusion involved substitution and subsequent migration from site to site, basically there is no reason why diffusion through {110}-surfaces should not be as good as through{100}-surfaces. It therefore seems that the electrostatically 'neutral' structure of {100}-surfaces makes it particularly easy for Au^{3+} to diffuse through whereas the different structure of {110}-surfaces presents relatively high potential barriers. The problem may be related to such factors as are involved in ion chanelling.

The ionic radii of Mg^{2+}, O^{2-} and Au^{3+} are 0.66 Å, 1.32 Å and 0.85 Å respectively, and their electronegativity coefficients are 1.1, 3.4 and 2.9 respectively. Electronegativity differences are $X(O^{2-})-X(Mg^{2+}) = 2.3$ and $X(O^{2-})-X(Au^{3+}) = 0.5$. Au^{3+} is thus unlikely to go into MgO substitutionally. This is unlike Cu^{+} which readily goes substitutionally into AgCl because $X(Cl^{-})-X(Cu^{+}) = 1.2 = X(Cl^{-})-X(Ag^{+})$. Also Au^{3+} is a much larger ion than Mg^{2+}, again unlike Cu^{+} which is much smaller (0.72 Å) than the host cation Ag^{+} (1.26 Å). Thus the important conclusion is reached that in the present case Au^{3+} resides in

MgO interstitially. Even so, since gold is trivalent there must be adequate compensation for the extra charge. Two Au^{3+} interstitials will lead to one Mg^{2+} vacancy, the gold ions being in adjacent octahedral sites with a magnesium vacancy in between as long as there are no other factors affecting this obvious arrangement.

5.3 Hardness

As Table 5.1 shows, heat-treating with or without gold increases the hardness of crystals by 25-30 % which must be due in part to solid solution hardening and in part to precipitation hardening. Since all of the dislocations remaining at the end of the heat treatment are locked by decoration they would not take part in any plastic deformation at room temperature. These are standard results regarding any decoration in any material whatsoever.

The incorporation of gold is not reflected in hardness. Gold precipitates on cooling. The original impurity content was up to 0.1 % whereas gold-impurity cannot be more than a tenth of this. Consequently gold may not be expected to have much effect, if any, on hardness. On the other hand, as stated in the last section, decoration seems to be by gold particles so that we have somewhat conflicting observations here. Or, and this is more likely, the two-stage cooling overages the crystals in the presence of gold which clearly is not soluble in MgO.

5.4 Cooling Rate and Dislocation Configurations

It was mentioned in §3.3.2 that there was a distinct difference between the appearance of the dislocations in crystals which had been cooled a little more rapidly ($10^{\circ}C\ min^{-1}$) during the first stage of cooling and that of dislocations in crystals which had been cooled less rapidly ($5^{\circ}C\ min^{-1}$). This is consistent with the general observation in most materials that dislocations tend to be jagged if vacancies do not easily disappear from the surface, which condition would hold for rapid cooling, whereas they tend to be smoothly curved if vacancies have the facility to diffuse towards surfaces and disappear, which condition would hold for less rapid cooling (Nabarro 1967). It is rather strange that cooling rates of $5^{\circ}C\ min^{-1}$ and $10^{\circ}C\ min^{-1}$, which do not differ all that much really, should make a significant difference. One could have understood the difference if the cooling rates had been widely different, say $5^{\circ}C\ min^{-1}$ and $50^{\circ}C\ min^{-1}$. However, the observation stated has been made repeatedly, so it appears that at the temperature of gold-diffusion ($1350^{\circ}C$) this difference between the cooling rates is significant.

The second stage-cooling rates in the two cases were identical ($2^{\circ}C\ min^{-1}$, Chapter 2). Since the difference between the two cases is in dislocation configurations but not in the

quality and depth of decoration, we conclude that it is during the second stage of cooling, in both cases slower than the first, that decoration occurs. Decoration requires not only the nucleation but also growth of particles so that the much smaller rate of cooling in the decorating stage is a natural requirement. It is during the first stage that the configurations observed get stabilized by the operation of one or more of the following factors:

(a) the diffusion of gold ions (Au^{3+}) towards dislocations

(b) the diffusion of vacancies towards dislocations and their consequent climb

(c) interaction between dislocations and Au^{3+}, leading to changes in configurations from what is normally expected (cf Parasnis et al 1963)

(d) the glide of dislocations, on both {110} and {100} under the action of thermal stresses, one another's stresses and stresses set up by Au precipitation processes.

Holding the crystals at the high temperature for long periods of time is responsible for (i) the diffusion of gold into the crystals throughout the volume, and (ii) annealing out of a part of the original dislocation content. The mechanisms suggested in the next section

should thus be understood to be taking place during the first stage of cooling.

5.5 Eiffel Towers and Long and Narrow Loops

5.5.1 Vacancy condensation

Consider first the possibility of condensation of point defects into discs and subsequent formation of loops (§ 4.2.1). Such loops, having Burgers vector $(a/2)\langle 110\rangle$ or $a\langle 100\rangle$ (Zakharov *et al* 1975 and Narayan 1978a), would be square-shaped or circular. Even after some glide, assuming they were glissile (which they are not), they would not have the long and narrow form. We may therefore discard point defect-condensation as the basic factor.

The next kind of mechanisms to consider is the formation of dipoles and subsequent pinching (§ 4.2.2). If the dipole is formed by the cross slip of a screw dislocation according to $\{110\}\langle 1\bar{1}0\rangle$ the subsequent pinching by another cross slip gives rise to a prismatic loop on $\{110\}$ elongated along $\langle 001\rangle$ that is like the loop L2a (Table 3.2 and Figure 5.1). Such a loop is known to break up into a string of circular loops thus reducing the energy considerably (Groves and Kelly 1962). This breaking up is not observed in the present work. If similar double cross slip mechanisms are to be invoked for the formation of the loops L1a,b and L2b a moment's thought will show that it is

necessary to invoke not only {100} slip planes but also a<100> Burgers vectors. We believe that such an abundance of slip-planes-and-vectors combination is unlikely to exist. We must therefore look for some other mechanism.

5.5.2 Dislocation collisions

Applying any of Tetelman's mechanisms (1962) of collisions between moving dislocations in order to have a variety of planes and directions of elongation in the end products is a formidable task. It will not be undertaken here, not because of its complexity but because it turns out that all manner of slip planes and vectors will have to be invoked here also. Although in recent times, as mentioned above, a<100> Burgers vectors have been observed the loops concerned are sessile so that it is not possible to visualize Tetelman's mechanisms operating with such a Burgers vector.

5.5.3 Slip loops

It is tempting therefore to give up the notion that the loops (L1, L2) are prismatic and consider them to be slip loops, the Burgers vector in each case being in the loop plane. Such an analysis has been done on the basis of a gliding screw dislocation (a/2)<110> coming across an obstacle, in particular a precipitate particle, forming a

dipole by wrapping itself around the obstacle and eventually pinching off, leaving behind a long and narrow loop (vide Orowan 1954b). Purely geometrically, all four loops can be formed in this way. Unless decoration starts immediately, thus locking a loop, the loop will not be long and narrow but more or less circular with the precipitate particle in the middle. While it is not possible to exclude this ideal sequence (the formation of a dipole, then of a loop and then immediate decoration) such a set of happenings seems somewhat artificial. Further, and this is a serious objection, the details of the crystallography of Eiffel towers on {110}-planes are inexplicable if all long and narrow loops were formed by this mechanism, for it seems that the origins of the two entities are the same (see remarks in this connection in Chapter 3). On the other hand, the towers entirely lying in {100} (Figures 3.5b, 3.10, 3.11) could be said to have formed in this way. It cannot be overemphasized that {100}-towers are entirely different from the {110}-towers. We shall use the term 'Eiffel Tower' for the latter only.

5.5.4 Mechanism suggested

Having discarded all existing possibilities we now suggest a mechanism which we think is consistent with all of the features observed. At the outset we assert that the upper

part of the Eiffel tower is a dislocation dipole because of its typical shape. It may be re-emphasized that these dipoles cannot have been produced by pure climb. In order for the reader exactly to follow the sequence of happenings we shall describe the mechanism stage by stage. Figure 5.1 is included for quick reference. Figure 5.2 indicates the coordinate system for working out indices of planes and directions. Some relevant planes and directions are also shown.

Stage 1 : To start with, an edge dislocation with its length along [011] is formed corresponding to the slip system (100) [0$\bar{1}$1] as shown in Figure 5.3a. Its half plane is (0$\bar{1}$1), ie the inclined plane of the diagram, to its right. The Burgers vector (a/2)[0$\bar{1}$1] is upwards.

Stage 2 : The straight dislocation takes a zigzag shape, its component segments being along [211] and [$\bar{2}$11] as shown in Figure 5.3a. (It is not implied that the dislocation has moved in (0$\bar{1}$1).) We have seen in Chapter 1 that edge dislocations along <112> with Burgers vector (a/2)<110> are configurationally charged and that in usual circumstances there would be no reason for them to assume this orientation and thus increase the energy of the crystal without compensating advantages. Since, however, in these crystals aliovalent ions Au^{3+} are present the dislocations are induced to take up this

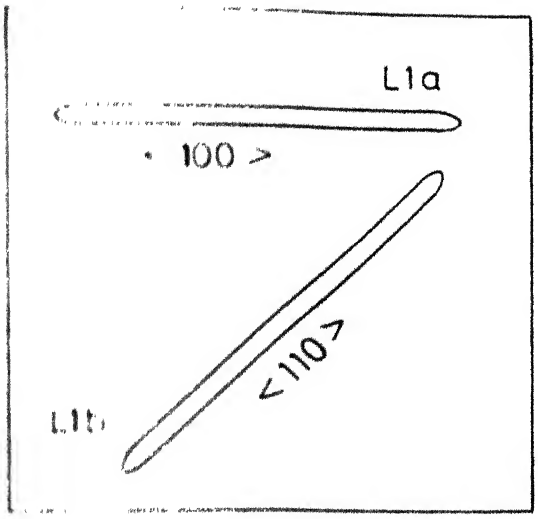

(a) {001}

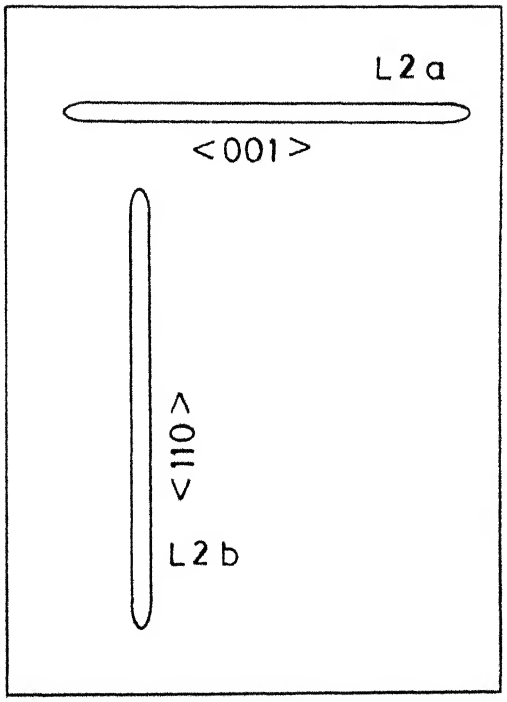

(b) {110}

Figure 5·1

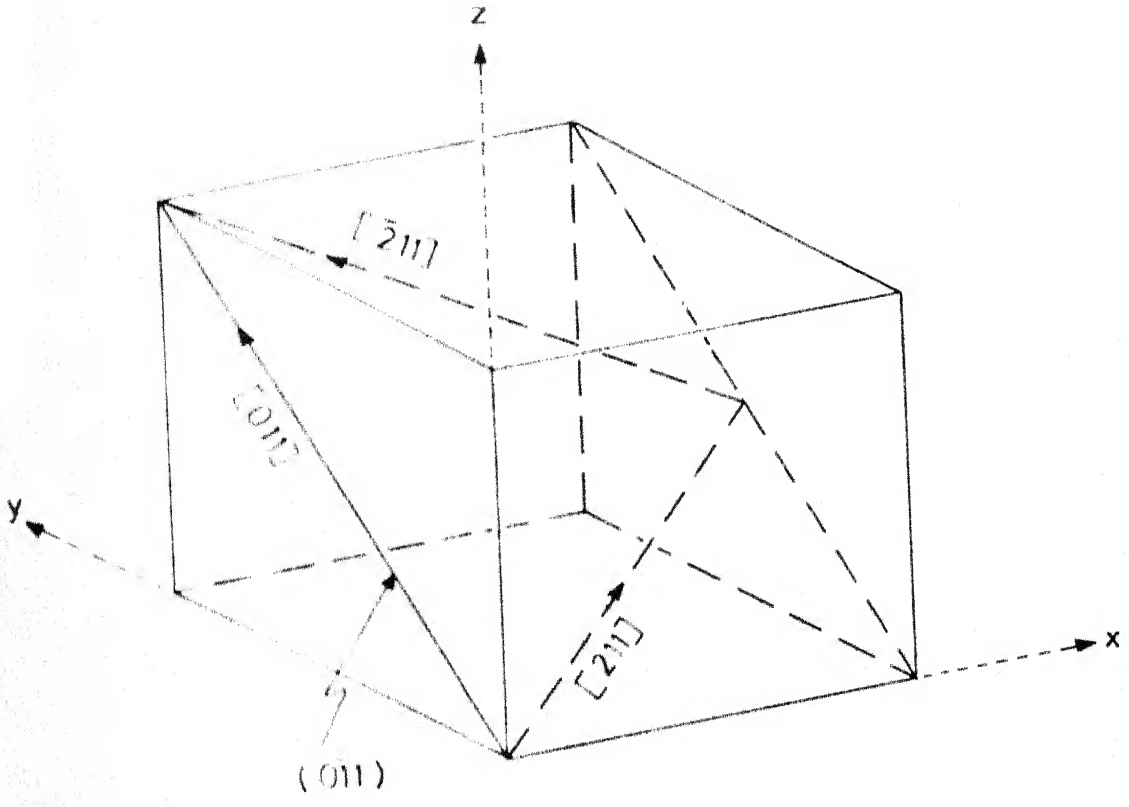

Figure 5.2

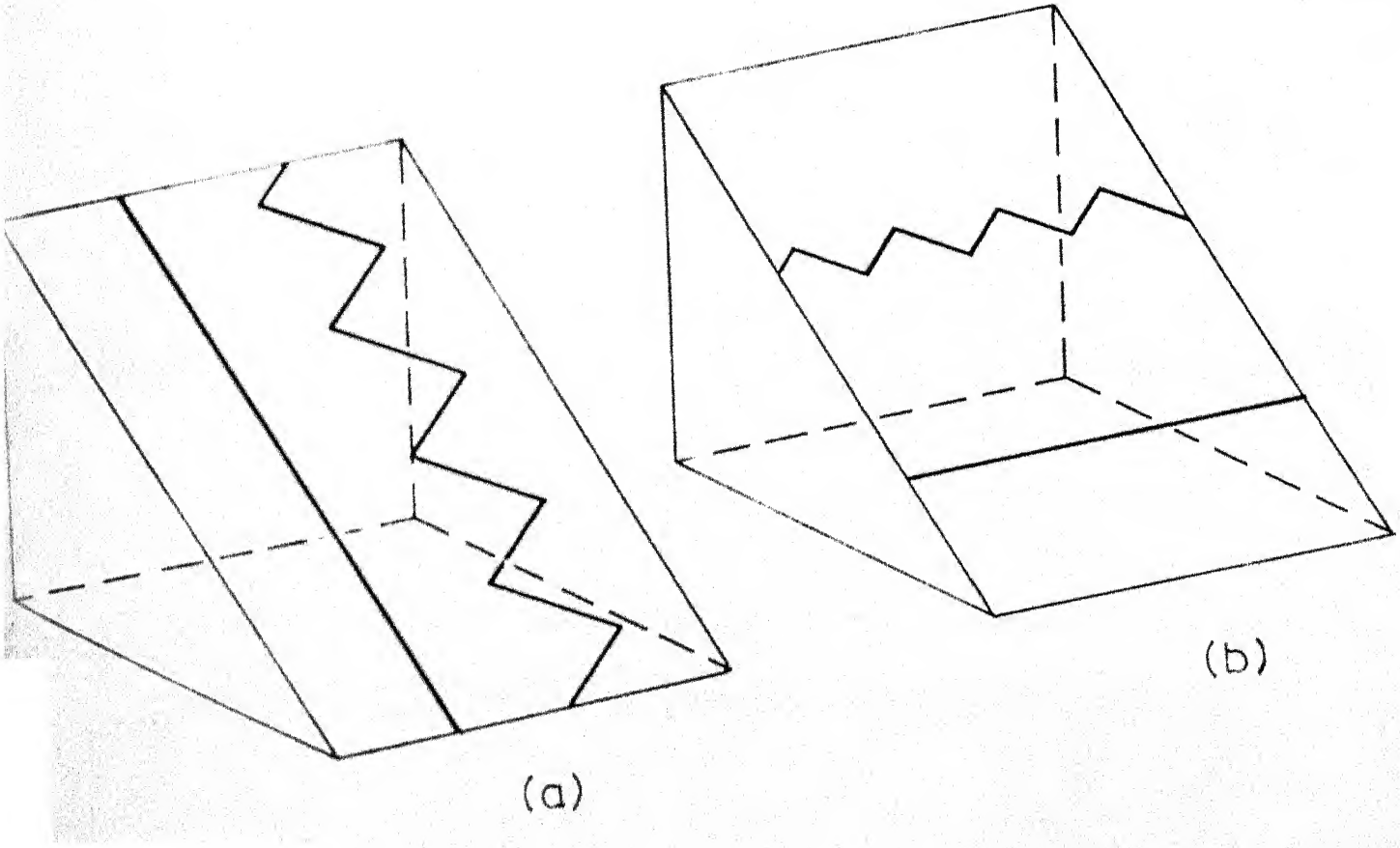

Figure 5.3

orientation and actually reduce the electrostatic energy of a cloud of Au^{3+} in the way described by Parasnis *et al* (1963). It was established in §5.2 that Au^{3+} ions reside interstitially. The compensating charge-cloud here therefore resides at the edge of the half plane which now is zigzag, preferably on the tension side where the interstitial volume is greater and may be compared loosely with the Cottrell atmosphere of (neutral) carbon atoms around dislocations in steel. At this stage the zigzagged dislocation is not completely locked by the charge-cloud because the temperature is sufficiently high for the individual ions in the cloud to migrate from one interstitial space to another should the dislocation for some reason glide along the {111}-slip planes. The activation energy for this migration is provided by the thermal vibrations of the lattice ions constituting the core of the dislocations and its immediate surroundings. Had the gold ions gone into the lattice substitutionally this would not happen and the dislocation would be more or less locked. The charge-cloud of interstitial gold ions propounded here also would lock the dislocation at room temperature since not enough thermal energy is available*

*The suggestion of the interstitial charge-cloud and the possibility of the combined entity moving through the crystal at high temperatures, and that of this combined entity being looked upon as an electrostatic dipole (§5.5.6) are due to Professor A S Parasnis. I am grateful to him for allowing me to make use of them here freely.

Stage 3 : At the end of the last stage the straight dislocation has become zigzag. During this stage adjacent zigs ([211]) and zags ([$\bar{2}$11]) separate away from each other in the direction of the Burgers vector. This motion is equivalent to a glide along their respective slip planes (11$\bar{1}$) and (1$\bar{1}$1). The [211]- and [$\bar{2}$11]-segments are now connected by short segments in screw orientation, alternately left- and right-handed. Figure 5.4 shows the shape of the dislocation at this stage (imagining, for the moment, the dipoles and loops to be retracted). It is seen that the dislocation has taken the shape of a flattened helix, the dimension along the direction [0$\bar{1}$1] being quite small. The helix is right-handed if [211]-segments move upwards relative to the [$\bar{2}$11]-segments, and left-handed if *vice versa* as shown in the figure. Helical dislocations have been proposed/observed in the case of a variety of materials during the last twenty and odd years. Apart from the flattened shape of this helix there are other important differences between it and the others: this helix arises from an edge dislocation rather than a screw and its Burgers vector is normal to its axis rather than along it. The zigzag dislocation taking up this helical configuration is an essential part of the mechanism being suggested and it is necessary to specify the cause of it. This matter is discussed in detail in §5.5.6.

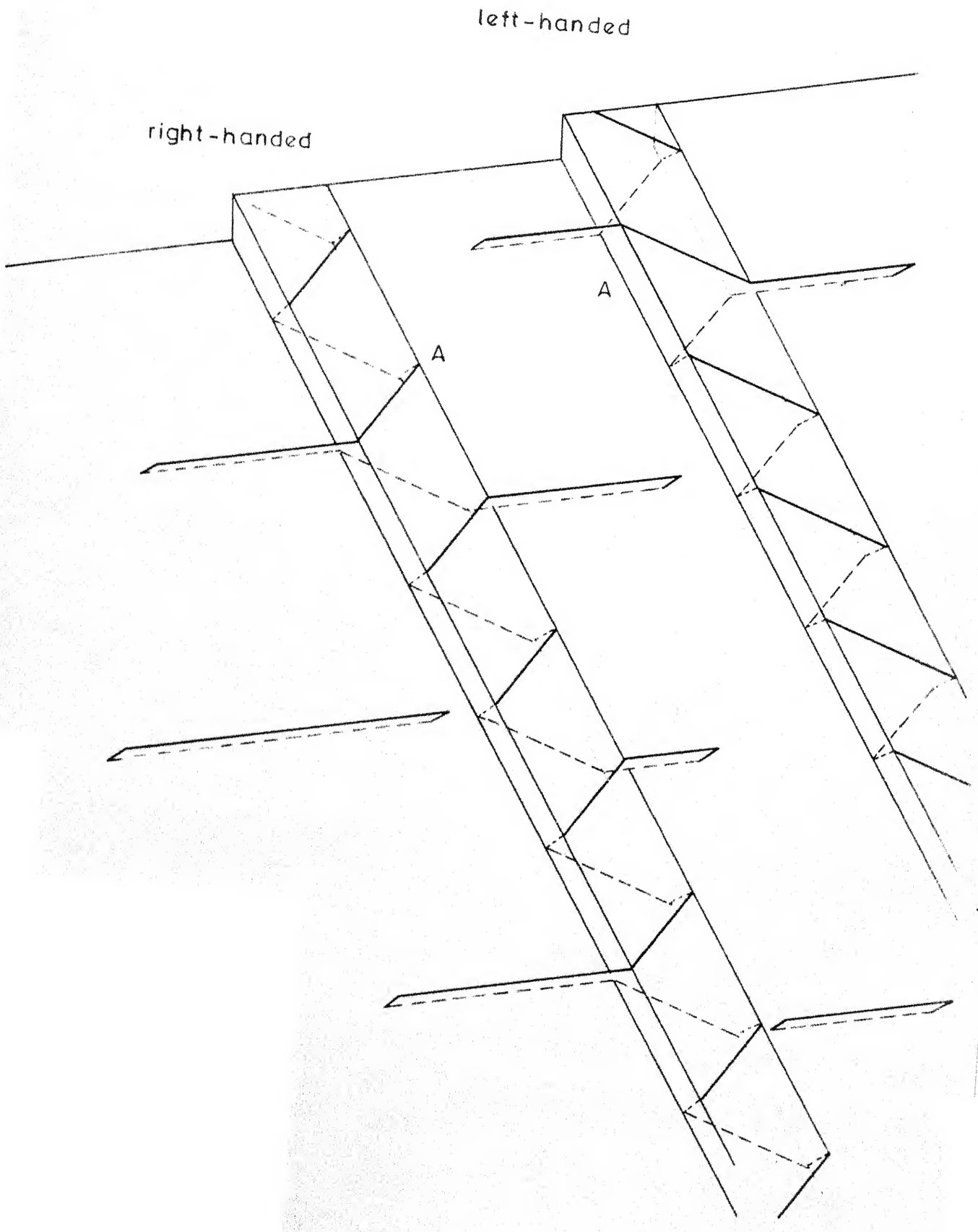

Figure 5.4

Figure 5.4 is not intended to imply that regular helices with so many turns are actually seen; rather, what is seen, as the photomicrographs of Chapter 3 show, is helices with two, three or four turns and these are seen throughout a crystal. The zigzag dislocation of Figure 5.3a and the helical dislocation of Figure 5.4 are drawn with a uniform width in the (011)-plane; it is clear that these are schematic diagrams and that in fact the width could be different in different parts.

Stage 4 : This is the stage during which dipoles are formed by the glide on (011) of the short screw segments as shown in Figure 5.4. Since there is no correlation among the instants when different screw segments may start gliding, the lengths of the dipoles by the time everything is immobilized by decoration are not the same; this is clearly seen in the photomicrographs of Chapter 3. The cause of this glide could be thermal or other stress. The line of sight being $[00\bar{1}]$ the dipoles on both sides of both left- and right-handed helices will be seen as having a small but definite width as shown in Figure 5.5a which is a projection on (001) of the structures seen at A in Figure 5.4. The crossing of the <112>-segments of a dipole is clearly seen in the photomicrograph of Figure 3.7. All of the dipoles of Figure 5.4 are in {110} with lengths parallel to <001>. Using the expression given in §4.2.2, viz

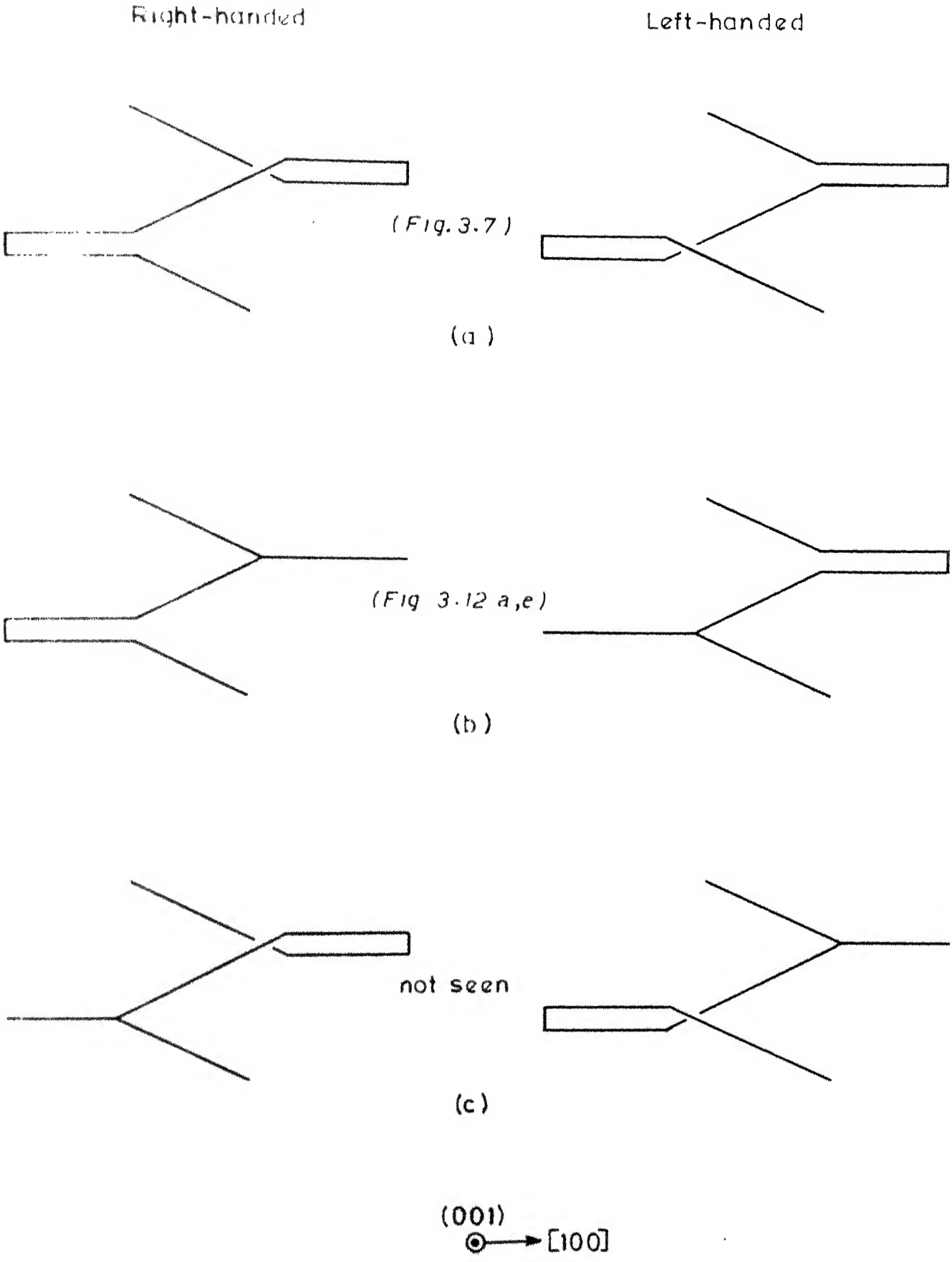
Right-handed
Left-handed
(Fig. 3.7)
(a)
(Fig 3.12 a,e)
(b)
not seen
(c)
(001)
[100]

Figure 5.5

$\tau \leq Gb/\{8\pi(1-\nu)h\}$

and putting in the values $G = 1.2 \times 10^4$ Kg mm^{-2}, $b = 4.2/\sqrt{2}$Å $\nu = 0.4$ and $h = 1.6$ μm we get $\tau \sim 1.45 \times 10^7$ dy cm^{-2}. If the thermal stress is about this value the dipole is stable enough.

Stage 4a : If instead of gliding in (011) the short screw segments glide in (100), dipoles lying on (100) with length along [011] will be produced (Figure 5.6).

Stage 5 : This stage effectively consists in the rotation of the plane of the dipole around its symmetry axis. The process is shown in Figures 5.7, 5.8a,b. Figure 5.8a shows the rotation of a dipole on the right hand side of the right-handed helix of Figure 5.4 and 5.8b shows that of one on the left. (Similar diagrams are easily drawn for the dipoles of the left-handed helix.) d-d represent the dipole before rotation. As a result of vacancies migrating to the dislocation core the half planes shrink and the two dipole segments travel towards d', d'. Eventually they align themselves along d'-d', which is the trace of the dipole plane, (010) in Figure 5.8a and (001) in Figure 5.8b. The former is seen edge on so that the appearance is as shown in Figure 5.5b and as seen in the photomicrographs of Figures 3.12a,c,e, whereas the latter is seen broadside on so that the full width is seen

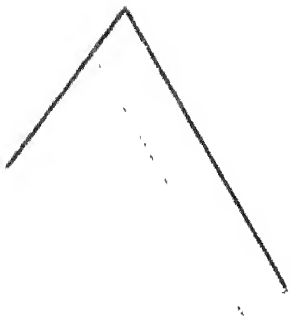

Figure 5.6

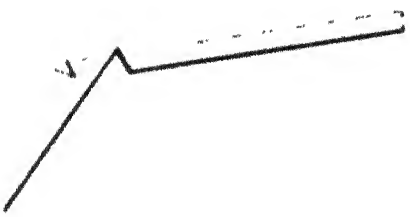

Figure 5.7

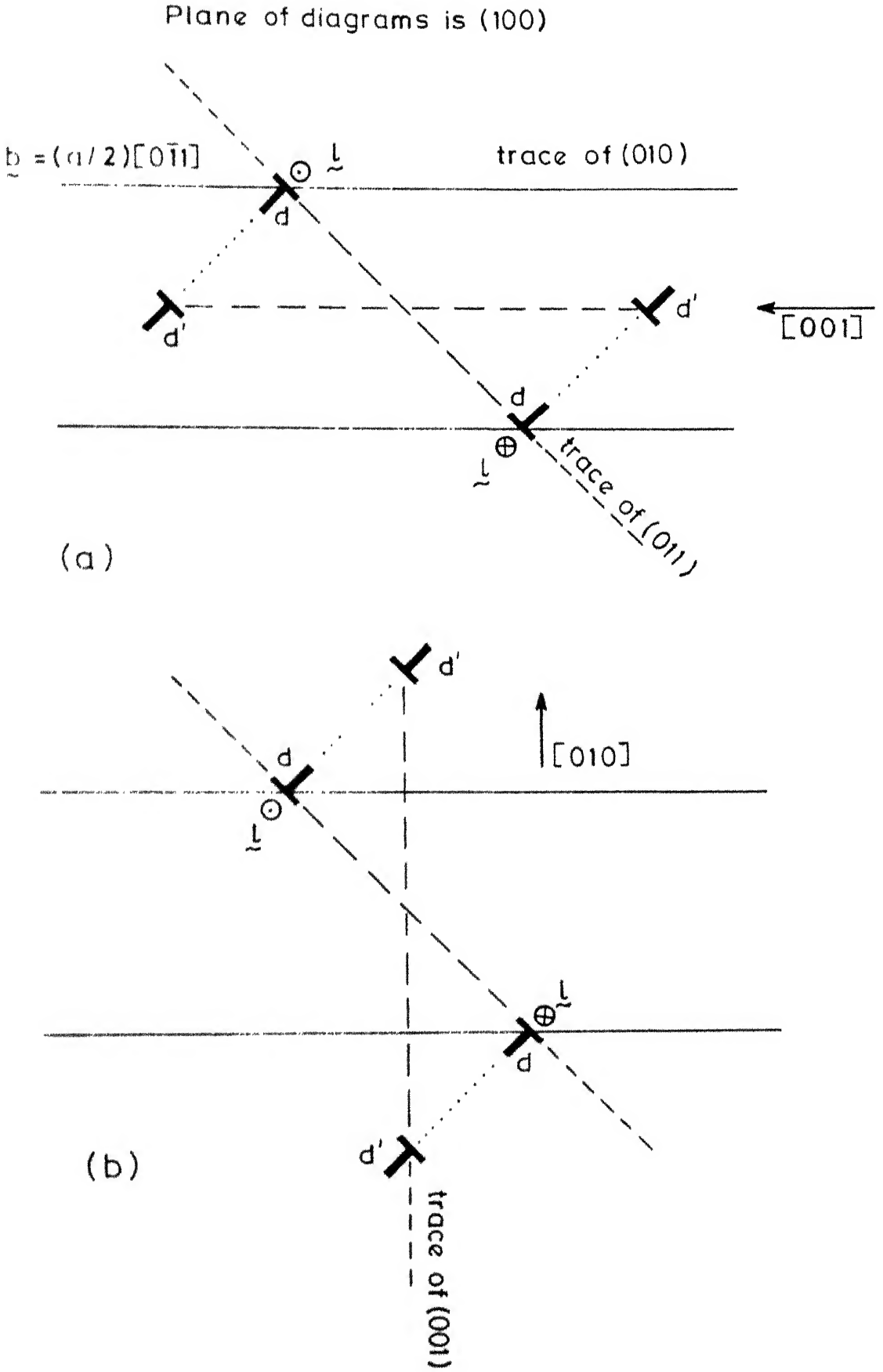
Plane of diagrams is (100)
b = (a/2)[0$\bar{1}$1]
l
trace of (010)
d
d'
d'
[001]
d
trace of (011)
(a)
d'
[010]
d
l
l
d
d'
trace of (001)
(b)

Figure 5·8

(Figures 5.5b and 3.12a,b). If the rotation had taken place due to the half planes of d,d extending due to interstitials, the appearance would be that of Figure 5.5c; this, however, is never observed - which is not surprising at all.

Stage 6 : It is during this last stage that the long and narrow loops are formed by the pinching of the dipoles. The pinching of dipoles at the end of Stage 4 presents no problems. Kinks of opposite sign are formed in the slip plane, viz (101), and pinching takes place in the usual way, giving the loops L2a. Soon after, decoration occurs which makes a loop not only visible but also immobile. In fact it is possible that decoration of the tip of the dipole has already started before pinching is complete. This would give the loop a somewhat tapering appearance. If decoration starts and immobilizes both the loop and its <112>-legs before pinching is complete, the situation would be as seen in the photomicrographs of Figure 5.7a,b.

On the other hand, if the loop plane has effectively rotated as described under Stage 5 and pinching occurs later, we would get loops L1a. The details of the actual pinching involved here are rather difficult to visualize for the geometry is complicated (Figure 5.7). The pinching of dipoles leading to the formation of loops is a process of

such common occurrence that we believe that even with this complicated geometry pinching somehow occurs resulting in loops L1a.

5.5.5 Loops L1b and L2b

We suggest the following two possibilities for dipoles corresponding to loops L1b and L2b to form. It was mentioned in stage 4a that the short screw segments of Figure 5.4 may glide along the direction [0$\bar{1}\bar{1}$] (see Figure 5.6). The resulting dipoles and eventual loops will be L2b. If rotation of the dipole plane occurs (by climb) before pinching, the loop will be L1b.

Another possibility is shown in Figure 5.3b. The starting configuration is a straight edge dislocation, length parallel to [100], corresponding to the slip system (011) [0$\bar{1}$1]. It becomes zigzag as shown in the same figure and follows the same stages as described in §5.5.4, mutatis mutandis.

Note that during the stages 4, 5 and 6 the <112>-segments remain anchored. The reasons are discussed in the next section.

5.5.6 Equilibrium of the helix of figure 5.4

We shall now discuss the question of why the zigzag dislocation starts taking the helical form and when the relative

movement of adjacent <112>-segments stops. The negatively charged [211]-- and [$\bar{2}$11]-dislocation segments and their associated positive charge-clouds of Au^{3+} ions may be looked upon as constituting continuous distributions of miniature electrostatic dipoles directed along [$\bar{1}$11] and [$\bar{1}\bar{1}\bar{1}$] respectively. In a two-dimensional problem this would give rise to a repulsive interaction in the plane of the zigzag dislocation (0$\bar{1}$1) only. Since, however, the (0$\bar{1}$1)-- planes above and below the nominal plane of the dislocation are bent the problem is a three-dimensional one. The point to note is that the interaction is repulsive in either case and in the latter has a force component along the direction of the Burgers vector. The adjacent segments must separate thus giving rise to the helix. As the segments separate, short screw segments appear and the strain energy increases. Although it is difficult without making a calculation, however rough, to estimate the energy it is evident that at some point the strain energy increase will compensate exactly the decrease in the electrostatic potential energy. The relative movement then stops and the helix is in equilibrium.

If any of the short screw segments starts gliding before the equilibrium is reached that portion of the helix would be stabilized against further separation. Incidence of decoration anywhere also would have the same effect.

The zigzag dislocation of Figure 5.3 has never been observed and the question may be asked why. This fact in itself seems to support the idea that adjacent <112> segments do separate as soon as they are formed.

5.6 Other Features

5.6.1 Spikes

One possibility for the formation of the Eiffel tower-like spikes (long or short, single or in sequence) was mentioned at the end of §5.5.3. Another is the mechanism of pure climb suggested by Miles (1965).

5.6.2 Lenticular loops and helix

Since the axis of the lenticular loop or of the corresponding helix of Figure 3.26 is along <110> such loops are prismatic and have been well known in many other materials also for many years. The helices arise from screw dislocations by jogging and stretching mechanism originally suggested by Seitz and later elaborated by Weertman (1957), Nash (1958), etc.

5.6.3 Straight-segmented loops

It has been established in Chapter 3 that the planes of straight-segmented loops are {110} but that their sides do not seem to correspond to any simple crystallographic directions. The loop in the photomicrograph of Figure 3.25

seems about to be pinched off and its sides, while seeming to form a parallellogram, are not quite straight. It seems then that the loop is pinched off (by whatever mechanism) first and that the straight segments develop later. The nearest crystallographic directions which at least approximately make with each other the correct angle are <116>. Referring to the structure of the {110}-planes one can see that a dislocation lying along <116> is likely to be charged. We wonder if it is not possible to describe them in the same way as dislocations lying along <112>. They seem to be prismatic, with $\underset{\sim}{b}$ normal to the loop-plane. These loops have not been investigated in detail.

5.7 Concluding Remarks

It will thus be seen that the major class of configurations observed in gold-doped single crystals of magnesium oxide, suitably heat-treated, namely the Eiffel towers and long-and-narrow loops, are suggested to have formed basically as a result of straight dislocations taking a charged zigzag shape in the presence of Au^{3+} ions. The mechanism suggested in § 5.5.4 might appear at first sight to be very complicated. Once, however, the interstitial charge-cloud and its properties are accepted it is only a sequence of simple stages. Our only apology, if one is needed, for it is that it explains very plausibly all of the features of these configurations.

The as-received crystals from either Semi-Elements or Ventron were admittedly impure at least to the certified 0.1%. Doubts may be raised as to the effect of these impurities on the whole concept of the charge-cloud neutralising the oppositely charged dislocation. The crystallography of the Eiffel towers and related loops (L1, L2) is such, we believe, as to leave no option but the mechanism suggested. The electron microscopic observations [illegible] should throw further light on the observations and discussions in this Report.

Appendix A

PLATELETS

It was mentioned in Chapter 3 that a large number of crystallites were observed on the surface of the heat-treated, gold-diffused specimens. When the specimens were mounted some of these platelets got detached from the surface and were seen suspended in the balsam away from the specimen. Figure A.1 shows some of these platelets having different shapes. Vast majority of such platelets observed were of rhombus-shaped. A few of them are shown in Figure A.2. Since most of the platelets were suspended it was difficult to locate perfectly flat ones. Hence these platelets were isolated from the specimen. All these platelets exhibited birefringence. They were observed consistently in a number of cases irrespective of the type of heat treatment to which the crystal was subjected to or the orientation of the heat-treated crystal. The angles of the opposite corners of the platelets were measured and the average of these angles was found to be $71^{\circ}49'$. Figures A3 and A4 show the same set of platelets seen under phase-contrast and dark-field illumination.

Figure A.1

Figure A.2

Figure A.3

Figure A.4

From the thermal history of the crystals these platelets were presumed to be of some gold chloride. In an attempt to identify them an EPR spectrum of these platelets was recorded in a Varian X-band EPR spectrometer at room temperature. But no signal was observed. The electronic configuration of atomic gold is Xe $4f^{14}5d^{10}6s^{1}$. Therefore the monovalent gold (Au^{+}) will have a completely filled outermost shell ($5d^{10}$) and hence it is not paramagnetic. But the trivalent gold (Au^{3+}) has an incomplete shell ($5d^{8}$). Therefore Au^{3+} is paramagnetic and hence it should give an EPR signal. But the negative result does not at once rule out the possibility of their being $AuCl_3$ crystals because we could not record the EPR spectrum at low temperatures. Since no literature was available about EPR studies on gold, further attempts to identify the platelets by EPR was given up. No further studies were carried out on these platelets since our major interest was on dislocation configurations.

——oOo——

REFERENCES

Amelinckx S (1957) 'Dislocations and Mechanical Properties of Crystals' ed Fisher J C et al (Wiley: New York) 3; (1964) 'Direct Observation of Dislocations' Solid State Physics Suppl 6 85

Appel F, Bethge H and Messerschmidt (1977) Phys Stat Sol A 42 61

Arain I and Hall L (1960) J Phys Chem Solids 29 335

Argon A S and Orowan E (1964a) Phil Mag 9 1003; (1964b) ibid 1023

Atkins A G and Tabor D (1967) J Am Ceram Soc 50 195

Bartlett J T and Mitchell J W (1958) Phil Mag 3 334

Bowen L H (1963) Trans Brit Ceram Soc 62 771

Bowen D H and Clarke F J P (1963) Phil Mag 8 1257

Brookes C A and Moxley B (1968) Am Ceram Soc Bull 47 349; (1975) J Phys E 8 456

Brookes C A, Bernard R P and Morgan J B (1975) J Mater Sci 10 2171

Buerger M J (1956) Am Minerologist 15 326

Clarke F J P, Bambell R A J and Tattersall H G (1962) Phil Mag 7 393

Dash W C (1958) Phys Rev Lett 1 400

Day R B and Stokes R J (1964) J Am Ceram Soc 47 493

De Batist R, Von Lingen E, Martyshev Yu N, Sil'vestrova I M and Urusovskaya A A (1968) Sov Phys-Crystall 12 881

Elkington W E, Thomas G, and Washburn J (1963) J Am Ceram Soc 46 307

Evans A G and Langdon T G (1976) Prog Mater Sci 21 No 3/4

Fishbach D B and Nowick A S (1955) Phys Rev 99 1333

Fontaine G (1968) J Phys Chem Solids 29 209

Fontaine G and Beason P (1969) Phys Stat Sol 31 K67

Fotedar H L, Srinivasan M, Wilson D A and Stoebe T G (1971) Mater Sci Eng 7 272

Fourie J T and Wildorf H G F (1960) J Appl Phys 31 2219

Friedel J (1964) 'Dislocations' (Pergamon Press: Oxford)

Gulanianvili N V (1970) Sov Phys-Sol State 12 987

Groves G W and Kelly A (1961) Phil Mag 6, 1527; (1962) J Appl Phys Suppl 33 456, (1962) Phil Mag 7 892 (erratum); (1963a) J Appl Phys 34 3104; (1963b); Phil Mag 8 877; (1963c) ibid 1437

Hauser J H and Mitchell J W (1953) Phil Mag 44 223

Henderson B (1964) Phil Mag 9 153

Hirth J P and Lothe J (1968) 'Theory of Dislocations' (McGraw-Hill: New York)

Huntington H B, Dickey J E and Thomson R (1955) Phys Rev 100 1117

Johnston T L, Stokes R J and Li C H (1962) Phil Mag 7 23

Johnston W G and Gilman J J (1960) J Appl Phys 31 632

Koh A S (1960) J Appl Phys 31 1538

Kocks U F (1966) Acta Met 6 85

Koehler J S (1952) Phys Rev 86 52

Lang A R and Miles G D (1965) J Appl Phys 36 1803

Langguon T G and Pask J A (1970) 'High Temperature Oxides' Vol 5 Part III ed Alper A M (Academic Press: New York) p 55

Li J C M and Swann P R (1964) Phil Mag 10 617

Miles G D (1965) J Appl Phys 36 1471

Mitchell J W (1962) J Appl Phys Suppl 33 406

Mitchell T E, Bernard R S, Howitt D G and Hobbs L W (1977) Proc 5th Int Conf HVEM, Kyoto, Japan Aug 29-Sept 1

Nabarro F R N (1967) 'Theory of Crystal Dislocations' (Oxford University Press: London)

Narayan J (1972) Phys Stat Sol B 54 K1; (1973a) J Appl Phys 44 2449; (1973b) ibid 44 3436; (1973a) Phys Stat Sol A 17 625; (1973b) Phil Mag 37 571

Narayan J and Washburn J (1972a) Script Met 6 263; (1972b) Cryst Lattice Defects 3 91; (1972c) Phil Mag 26 1179; (1972d) J Appl Phys 43 4862; (1973) Acta Met 21 533

Orowan E (1966a) Phil Mag 13 1097; (1966b) ibid 14 619

Orowan E (1954a) 'Dislocations in Metals' 69; (1954b) ibid 103

Parmanis A S (1960) Ph D Thesis (Bristol); (1979) To be published

Parmanis A S and Mitchell J W (1959) Phil Mag 4 171

Parmanis A S, Frank F C and Michell J W (1963) Phil Mag 8 1053

Parmanis A S, Singh R P and Swamy Rao K N (1973) Ind J Tech 11 407

Price P B (1960) Phil Mag 5 873

Queen F and Dekeyser W (1961a) J Appl Phys 32 1799; (1961b) Phil Mag 6 359

Singh K N and Coble R L (1974) J Appl Phys 45 990

Smoluchowski R (1966) J Phys 27 Colloque C3 3

Sprackling M T (1976) 'The Plastic Deformation of Simple Ionic Crystals' (Academic Press: New York)

Stepanov A V (1933) Z Phys 81 560

Stokes R J and Li C H (1964) Discuss Farad Soc 38 233

Stokes R J and Olsen K H (1963) Phil Mag 8 957

Tetelman A S (1968) Acta Met 10 813

Venables J A (1963) Phys Rev 122 1388; (1963) J Appl Phys 34 293

Washburn J (1963) 'Electron Microscopy and Strength of Crystals' ed Thomas G and Washburn J (Interscience: New York) 361

Washburn J, Kelly A and Williamson G K (1960a) Phil Mag 5 192

Washburn J, Grove G W, Kelly A and Williamson G K (1960b) Phil Mag 5 991

Washburn J and Cass T (1966) J Phys 27 Colloque C3 168

Weertman J (1957) Phys Rev 107 1259

Westwood A R C (1961) Phil Mag 6 195

Whitworth (1965) Phil Mag 11 83; (1975) Adv Phys 24 203

Wise E M (1964) 'Gold-Recovery, Properties and Applications' (D Van Nostrand: New York) 44

Zakharov N D, Kostner G and Rozhanski V N (1975) Sov Phys Solid State 16 1801